

# SOAR optical and near-infrared spectroscopic survey of newly discovered massive stars in the periphery of Galactic Massive star clusters I - NGC3603

A. Roman-Lopes

*Department of Physics and Astronomy – Universidad de La Serena, Cisternas 1200, La Serena, Chile*

`aroman@userena.cl`

G. A. P. Franco

*Departamento de Física – ICEx – UFMG, Caixa Postal 702, 30.123-970, Belo Horizonte, MG, Brazil*

D. Sanmartin

*Southern Astrophysical Research Telescope (SOAR), Chile*

## ABSTRACT

In this work, we present the results of a spectroscopic study of very massive stars found outside the center of the massive stellar cluster NGC3603. From the analysis of the associated SOAR spectroscopic data and related optical-NIR photometry, we confirm the existence of several very massive stars in the periphery of NGC 3603. The first group of objects (MTT58, WR42e and RFS7) is compound by three new Galactic exemplars of the OIf\*/WN type, all of them with probable initial masses well above  $100 M_{\odot}$  and estimated ages of about 1 Myrs. Based on our Goodman blue-optical spectrum of MTT68, we can confirm the previous finding in the NIR of the only other Galactic exemplar (besides HD93129A) of the O2If\* type known to date. Based on its position relative to a set of theoretical isochrons in a Hertzsprung-Russel diagram, we concluded that the new O2If\* star could be one of the most massive ( $150 M_{\odot}$ ) and luminous ( $M_V = -7.3$ ) O-star in the Galaxy. Also, another remarkable result is the discovery of a new O2V star (MTT31) that is the first exemplar of the class so far identified in the Milk Way. From its position in the Hertzsprung-Russel diagram it is found that this new star probably had an initial mass of  $80 M_{\odot}$ , as well as an absolute magnitude  $M_V = -6.0$  corresponding to a luminosity similar to other known O2V stars in the LMC. Finally, we also communicate the discovery of a new Galactic O3.5If\* star

(RFS8) which case is quite intriguing. Indeed, It is located far to the south of the NGC 3603 center, in apparent isolation at a large radial projected linear distance of  $\sim 62$  pc. Its derived luminosity is similar to that of the other O3.5If\* (Sh18) found in the NGC 3603’s innermost region, and the fact that a such high mass star is observed far isolated in the field led us to speculate that perhaps it could have been expelled from the innermost parts of the complex by a close fly-by dynamical encounter with a very massive hard binary system.

*Subject headings:* Stars: Individual: MTT31, MTT58, MTT68, MTT71, WR20aa, WR42e, HD93129A; Galaxy: open clusters and associations: individual: NGC 3603

## 1. Introduction

Very Massive Stars (VMS) (Vink et al. 2015) are expected to be found in the core of their host clusters, generally forming binary or multiple stellar systems. Indeed, it is well accepted that the majority of massive stars are formed in clusters with the O3 stars being considered for a long time, the most massive hydrogen core burning stellar type. However, the situation has changed in the last few decades, as we now know that some hydrogen-rich nitrogen sequence Wolf-Rayet (WR) stars are in reality extremely massive and luminous main-sequence (MS) stars, which because the proximity to the Eddington limit, mimic the spectral appearance of classical WR stars showing an emission-line spectrum even at the beginning of their main-sequence evolution (de Koter, Heap & Hubeny 1997; Schnurr et al. 2008; Smith & Conti 2008; Crowther et al. 2010).

Several observational studies on stellar masses of very massive binary systems, indicate that such massive stellar objects belong to the OIf\*/WNH and WNH spectral types (Smith & Conti 2008; Crowther et al. 2010; Crowther & Walborn 2011), making them the most massive MS stars known in the local universe. Evidence supporting this assumption come from systematic studies of binaries made by Rauw et al. (1996) for WR22 (minimum masses of  $71.7 \pm 2.4 M_{\odot} + 25.7 \pm 0.8 M_{\odot}$ ), Rauw et al. (2004) and Bonanos et al. (2004) for WR20a (two O3If\*/WN6 stars with absolute masses of  $83 M_{\odot}$  and  $82 M_{\odot}$ ), Niemela et al. (2008) for WR21a (a WN6ha star with minimum mass of  $87 M_{\odot} +$  O-type secondary with a minimum mass of  $53 M_{\odot}$ ), Schnurr et al. (2008) for NGC3603-A1 (minimum masses of  $116 \pm 31 M_{\odot} + 89 \pm 16 M_{\odot}$ ), Schnurr et al. (2009) for R145 (minimum masses of  $116 \pm 33 M_{\odot} + 48 \pm 20 M_{\odot}$ ). Finally, Crowther et al. (2010) found from their spectroscopic re-analyses of OIf\*/WN and WNH stars in the cores of NGC 3603 and R136 in the Large Magelanic Cloud (LMC), that some stars there might had initial masses in the range of  $105\text{--}170 M_{\odot}$ .

and 165-320  $M_{\odot}$ , respectively.

Surprisingly, some VMS are found in isolation in the field. As examples we can mention the cases of WR21a (a binary with minimum masses  $87 M_{\odot} + 53 M_{\odot}$  - Niemela et al. (2008)) in Westerlund 2 (Wd2), WR42e (an O3If\*/WN6 with estimated initial mass above  $100 M_{\odot}$  - Roman-Lopes (2012); Gvaramadze et al. (2013)) in NGC 3603, and VFTS 682 in the Large Magellanic Cloud (LMC) whose blue-optical spectra looks very similar to that of R136a3 (one of the WNH stars found in the centre of R136), with an inferred initial mass of  $\sim 150$ - $200 M_{\odot}$  - Bestenlehner et al. (2011); Vink et al. (2015)). In this sense, there is a growing number of VMS that are seen outside the cluster cores, sometimes found far away from their supposed parental clusters, perhaps forming massive stellar halos like the one seen in the field of the 30 Dor starburst region in the LMC (Walborn & Blades 1994; Walborn et al. 2014). In the Milk Way, this phenomenon seem to occur in the periphery of massive stellar clusters like Wd2 and NGC 3603, in which some of the most massive stellar members are found far from the cluster centers. For example, in Wd2 besides WR20a there are WR20b (WN6ha - Moffat, Shara & Potter (1991); Shara et al. (1991)) and WR21a (WN6 + early-O) (Niemela et al. 2008), which are found in isolation at angular radial cluster center distances ( $R_c$ ) of  $0.6'$ ,  $3.7'$ , and  $16'$ , respectively, plus two O2If\*/WN6 stars, WR20aa and WR20c (Roman-Lopes, Barbá & Morrel 2011), placed at large  $R_c$  values of  $15.7'$ , and  $25'$ , respectively. On the other hand, in the NGC3603's field there are three exemplars: MTT58 (O2If\*/WN6), MTT68 (O2If\*) and WR42e (O2If\*/WN6) at  $R_c$  values of  $1.0'$ ,  $1.4'$ , and  $3'$ , respectively (Roman-Lopes 2012, 2013a,b).

For comparison, in Table 1 it is shown the number of VMS found in the direction of Wd2 and NGC 3603, tabulated for  $R_c$  values in the ranges  $0 < R_c < r$ ,  $r < R_c < r_t$  and  $R_c > r_t$ , with  $r$  and  $r_t$  being the observed cluster radius and the cluster tidal radius, respectively, taken from Hur, Sung & Lim (2014) and Sung & Bessell (2004). We can see that the number

Table 1: Number of O2If\*, OIf\*/WN and WNH stars previously known in the Wd2 and NGC3603 fields, found at  $R_c$  distances in intervals  $R_1=(0 < R_c < r)$ ,  $R_2=(r < R_c < r_t)$  and  $R_3=R_c > r_t$ . The parameters  $r_c$ ,  $r$  and  $r_t$  are respectively the observed cluster core radius, the cluster radius and the cluster tidal radius of NGC 3603 and Wd2 derived by Hur, Sung & Lim (2014) and Sung & Bessell (2004).

Cluster	$r_c$ (')	$r$ (')	$r_t$ (')	[ 0 - r ]	[ r - $r_t$ ]	[ > $r_t$ ]
Wd2	0.2	1.78	4.8	1	1	3
NGC3603	0.05	2.0	14.6	7	1	0

of O2If\*, OIf\*/WN and WNH objects found inside the circular area limited by the cluster radius  $r$  is higher in NGC 3603 than in Wd2, perhaps reflecting differences in the total mass of each cluster and/or in their dynamical evolutionary stages. On the other hand, no such objects are found beyond the area projected by the respective tidal radius, a behavior that led us to wonder if there would be some other VMS still to be discovered in the outskirts of the NGC3603 complex.

In this work we performed a search for VMS candidates placed beyond the center of the massive stellar cluster NGC3603, which is known to be one of the most massive, dense and rich Galactic star-forming region (Melnick, Tapia, & Terlevich 1989; Moffat et al. 2002; Sung & Bessell 2004), and believed to be a scaled version of the star-burst R136 cluster in the Large Magellanic Cloud (LMC). It has several massive stars in its core, many of them apparently showing initial masses up to 100-170  $M_{\odot}$  (Crowther et al. 2010). Based on near-infrared (NIR) colour and magnitude selection criteria applied to objects found in the 2MASS point source catalogue - 2MASS PSC - Skrutskie et al. (2006), the chosen stars were surveyed through a SOAR NIR spectroscopic survey aimed to confirm their possible massive nature. The earliest stars selected from our analysis of the respective NIR spectra were then re-studied and spectroscopically re-classified using new SOAR-Goodman blue-optical data, resulting on the confirmation of the existence of several new massive stars in the NGC3603 field.

## 2. Near-IR magnitude and color-ratio selection criteria

The stars of this work were selected from the study of the near-infrared (NIR) magnitudes and colors of sources in the 2MASS PSC found on the annular sky area (centered on the NGC3603's coordinates) of internal and external radius 0.5', and 35', respectively, and presenting  $K_S$ -band magnitudes in the range  $8.5 < K_S < 10$  and magnitude errors  $< 0.1$ . For the sources matching the mentioned spatial and magnitude criteria, we kept those showing colors and color-ratios in the range  $0.5 < (J - K_S) < 1.5$  and  $1.5 < [(J - H)/(H - K_S)] < 2.0$ , respectively, which in turn were defined based on the fact that massive stars are known to emit a lot of excess of radiation in the infrared and radio domains, mainly due to the free-free emission generated by their powerful stellar winds (for more on this see Lamers & Cassinelli (1999) and references therein). In this sense, the  $K_S$ -band magnitude range and color criteria were tuned based on those of WR42e (O2If\*/WN6), MTT58 (O2If\*/WN6) and MTT68 (O2If\*), with the  $K_S$ -band magnitude limit ( $K_S=10$ ) being fixed considering the maximum integration time previously assigned per source (about 30-35 minutes) with OSIRIS at SOAR, taking into account a minimum  $S/N = 100$  in the same spectral band. This empirical limit

Table 2. List of stars observed with Osiris and Goodman with the SOAR telescope. Column 1 is the assigned ID, columns 2 and 3 their coordinates (J2000), columns 4 and 5 the B-, V-band photometry taken from Sung & Bessell (2004); Zacharias et al. (2004, 2013), columns 6-8 the J-, H- and  $K_S$ -band photometry taken from the 2MASS PSC. Column 9 the corresponding NGC3603 radial angular and projected linear distance (parsecs - assuming a heliocentric distance of 7.6 kpc (Crowther et al. 2010)) center distances, and column 10 the observed wavelength ranges. Finally, in column 11 we list the IDs of the sources found in the literature, as well as the objects with (when available) X-ray band measurements. The previously assigned IDs for some of the sources listed here (like RFS1, RFS2, RFS3, and RFS4) are from the work of Melnick, Tapia, & Terlevich (1989), while WR42e was previously named by Roman-Lopes (2013b). Also the informations on the X-ray source counterparts are from the catalog of Romano et al. (2008) (for RFS1 to RFS5), and in case of RFS10, from the XMM-Newton Serendipitous Source catalog (XMM-Newton Survey Science Centre 2013).

Source	RA(J2000)	Dec(J2000)	B	V	J	H	$K_S$	r (arcmin - pc)	OSIRIS Data	comments
RFS1	11:15:06.68	-61:16:33.3	15.29	14.07	10.67	10.17	9.86	0.7 - 1.5	Optical+NIR	MTT31 <sup>(1)</sup> (O4V-O5V and X-Ray)
RFS2	11:15:07.58	-61:16:54.6	16.14	14.76	10.47	9.68	9.24	1.0 - 2.1	Optical+NIR	MTT58 (X-Ray)
RFS3	11:14:59.48	-61:14:33.8	16.31	14.72	9.98	9.17	8.74	1.4 - 3.0	Optical+NIR	MTT68 (X-Ray)
RFS4	11:15:21.32	-61:15:04.3	16.31	14.74	10.60	9.99	9.60	1.8 - 3.7	Optical+NIR	MTT71 (X-Ray)
RFS5	11:14:45.50	-61:15:00.1	16.05	14.53	10.18	9.47	9.04	3.0 - 6.4	Optical+NIR	WR42e (X-Ray)
RFS6	11:14:53.55	-61:24:22.8	16.02	14.52	10.64	10.06	9.73	8.5 - 18	Optical+NIR	X-Ray source
RFS7	11:15:15.36	-60:51:17.6	14.17	12.89	9.85	9.39	9.12	25 - 53	Optical+NIR	—
RFS8	11:16:12.62	-61:43:54.2	15.31	14.68	10.61	9.92	9.48	29 - 62	Optical+NIR	—
RFS9	11:12:53.35	-60:50:45.2	14.98	13.62	10.55	10.06	9.83	30 - 64	Optical+NIR	—
RFS10	11:19:55.12	-61:16:03.7	15.21	13.86	10.54	10.03	9.66	35 - 74	Optical	X-Ray source

Note. — (1) Previous spectral type for MTT31 (RFS1) as presented by Moffat et al. (2002)

possibly results in a bias towards the most luminous (and potentially massive) objects, what in principle is not an issue as our main goal is to do it for the most promising candidates. In one hand, by using the mentioned magnitude limits we can probably be missing several mid- to late-O type stars. Indeed, as an example of this behavior we can mention the case of the newly discovered O6V runaway star 2MASS J11171292-6120085 (Gvaramadze et al. 2013) that is found at  $15.6'$  from the NGC3603's center, which is not selected by our methodology because its  $K_S$  magnitude (10.92) is well above the assumed upper selection limit. On the other hand, we are also probably missing a certain number of massive stars positioned in the innermost regions of the complex, e.g. those with radial distances  $r < 0.5'$ .

From the application of the above criteria, about thirty 2MASS point sources were selected. Two of them are the known WR stars WR42c and WR42d (both of the WN5 type (Rosslowe & Crowther 2015)), placed at NGC3603 radial distances of  $15'$  and  $6'$ , respectively. On the other hand, in the innermost regions there are two known O-stars, SHER 22 (O2-O3 III) and SHER 23 (OC9.7 Ia), both found at less than  $0.5'$  from the NGC3603 center. The ten most extreme objects of the remaining selected sources are the subject of this paper. Their coordinates and photometric parameters, together with the assigned spectral types and NGC3603 radial distances, are listed in Table 2. In Figure 1 we present a colorized Spitzer image centered on the NGC 3603 complex, in which we indicate the position of each selected source (shown by labels and arrows), as well as their relative position to NGC 3603, NGC 3576 and NGC 3590 star formation complexes.

Table 3. Journal of the SOAR spectroscopic data used in this work.

Night	UT	Seeing (")	Instrument	Mode	Slit	Resolving Power	Coverage
09-05-11	04:10:00-04:22:00	0.8-1.0	OSIRIS	XD - f/3	1"	1000	1.25-2.35 $\mu$ m
18-12-11	07:22:00-09:13:00	0.8-1.0	OSIRIS	XD - f/3	1"	1000	1.25-2.35 $\mu$ m
31-01-12	06:06:00-08:25:00	0.8-1.0	OSIRIS	XD - f/3	1"	1000	1.25-2.35 $\mu$ m
29-12-12	06:02:00-06:58:00	0.6-0.8	OSIRIS	XD - f/3	1"	1000	1.25-2.35 $\mu$ m
26-01-13	02:55:00-07:06:00	1.0-1.5	OSIRIS	XD - f/3	1"	1000	1.25-2.35 $\mu$ m
28-02-13	08:22:00-09:09:00	1.0-1.2	Goodman	GG385 - 600 l/mm	1.03"	1800	0.45-0.67 $\mu$ m
30-03-13	07:05:00-07:46:00	0.6-0.8	OSIRIS	XD - f/3	1"	1000	1.25-2.35 $\mu$ m
08-03-15	04:54:00-08:05:00	1.0-1.5	Goodman	930 - m2	1.03"	2100	0.39-0.55 $\mu$ m
28-03-15	02:15:00-05:16:00	1.0-1.5	Goodman	930 - m2	1.03"	2100	0.39-0.55 $\mu$ m
29-06-15	22:48:00-03:08:00	0.8-1.3	Goodman	930 - m2	1.03"	2100	0.39-0.55 $\mu$ m



Fig. 1.— A colorized Spitzer image (blue- $3.6\mu\text{m}$ , green- $4.5\mu\text{m}$ , red- $8.0\mu\text{m}$ ) in the direction of the NGC 3603 complex, in which we indicate the position of each source in our sample (shown by labels and arrows), as well as their relative position to NGC 3603, NGC 3576 and NGC 3590. North is to the top and east to the left. The approximate tidal radius (about 15 arcmin) area is indicated by the blue dotted line.

### 3. Spectroscopic data

In this section we present details on the observations and data reduction process of the Ohio State Infrared Imager and Spectrometer (OSIRIS) NIR and Goodman optical spectroscopic data taken at the Southern Astrophysical Research (SOAR) Telescope for sources listed in Table 2. All but one of them (RFS10), were observed with both instruments. Our strategy was to observe the sources selected from the photometric criteria, first through the NIR window using OSIRIS, because many of the science targets are relatively faint at the U- and V-bands, mainly due to the large heliocentric distances combined with heavier interstellar absorption. The typical integration time necessary to get a  $S/N \approx 100$  (at  $\approx 4800\text{\AA}$ ) for a science target with  $V=14-15$  (using Goodman at SOAR in a gray time night) is about 1.0-1.5 hours, while if we consider the  $K_S$ -band magnitude range as defined in Section 2.1, the necessary average exposure time with OSIRIS at SOAR (to get a  $S/N \approx 100$  in the  $K_S$ -band) drops to no more than 15 to 20 minutes.

#### 3.1. OSIRIS Near-infrared and Goodman Blue-optical spectroscopic dataset

The NIR spectroscopic data were obtained on observing runs (summarized on Table 3) during nights that in general presented good weather conditions. The raw frames were reduced following standard NIR reduction procedures, which are presented in details in Roman-Lopes (2009), and shortly described here. The two-dimensional frames were sky-subtracted for each pair of images taken at two nod positions, followed by division of the resultant image by a master flat. The multiple exposures were combined, and then followed by one-dimensional extraction of the spectra. Thereafter, wavelength calibration was applied using the sky lines and being conservative we estimate as  $\sim 12-16\text{\AA}$ , the  $1-\sigma$  error for such calibrations. This result comes from the fact that we considered the associated  $1-\sigma$  error as the mean values measured from the full width half maximum (FWHM) of the sky lines detected in all three NIR bands. On the other hand, if we instead assume the most common criterium of  $1/3$  of the observed FWHM, then the associated  $1-\sigma$  error drops to  $\sim 4-5\text{\AA}$ . Also, the effects of the earth atmosphere in the science spectra were corrected using J-, H- and K-band spectra of A-type stars, with the intrinsic hydrogen lines being carefully subtracted by modeling the observed line profiles through the use of Voigt profiles given by the SPLOT task on IRAF<sup>1</sup>. The final NIR spectra were normalized through the fitting to the continuum emission observed in the associated wavelength range. We notice that with the exception of RFS2, all sources in Table 2 were observed in the blue-optical window in March

---

<sup>1</sup><http://iraf.noao.edu/>



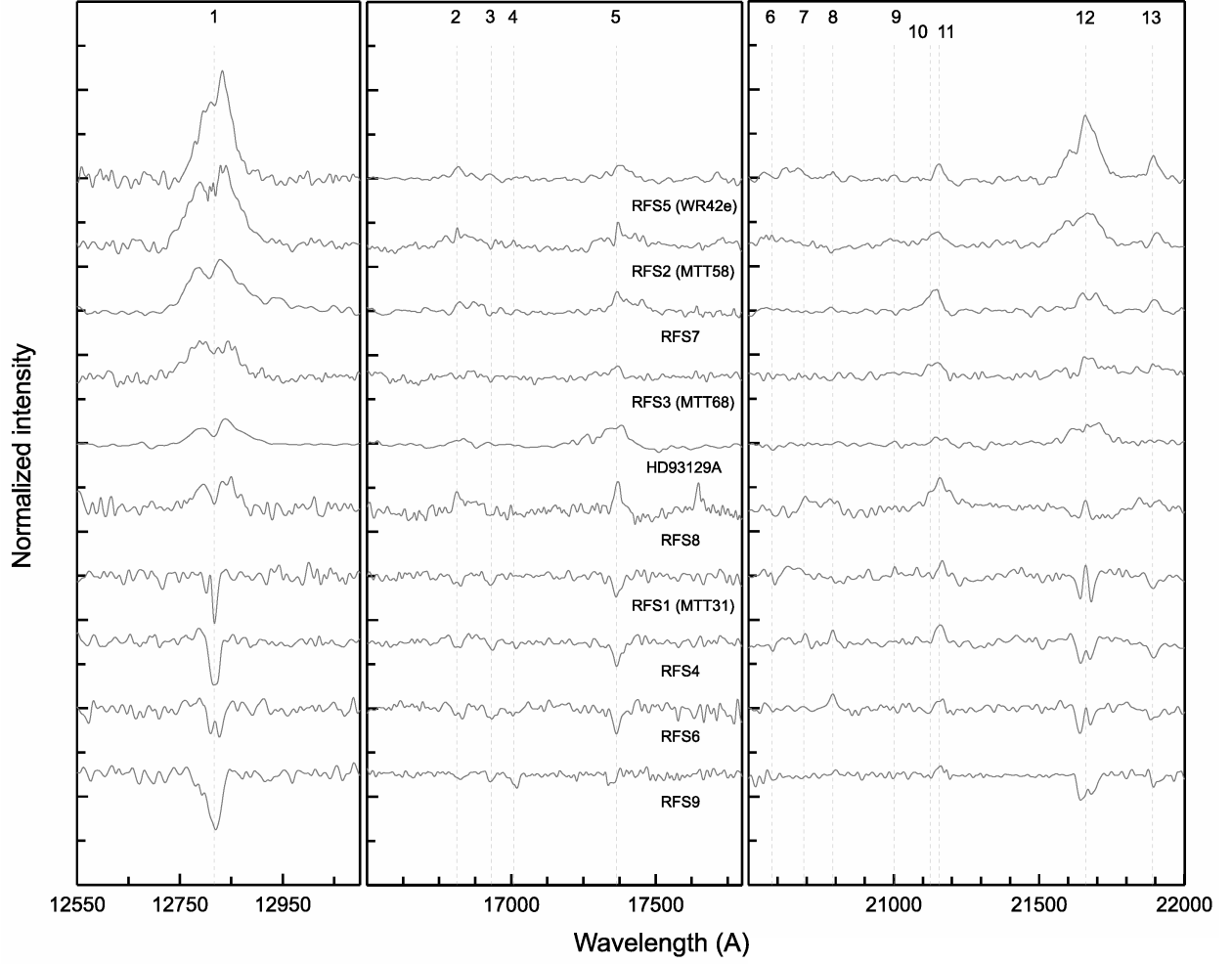


Fig. 2.— OSIRIS spectra of sources in Table 2. The main line features are indicated as follow: (1) Pa $\beta$   $\lambda$ 12822, (2) Br 11  $\lambda$ 16811, (3) He II  $\lambda$ 16930, (4) He I  $\lambda$ 17007, (5) Br 10  $\lambda$ 17367, (6) He I  $\lambda$ 20590, (7-8) C IV  $\lambda\lambda$ 20690-20802, (9) N V  $\lambda$ 21000, (10) He I  $\lambda$ 21126 (11) N III  $\lambda$ 21160, (12) Br $\gamma$ , (13) He II  $\lambda$ 21890.

2015, with the data being acquired using the 1.03'' long slit and the 930 - m2 (3850-5550Å) grating, which provides a maximum resolving power  $R \sim 2100$ . On the other hand, RFS2 was observed with Goodman in February 2013 using the GG385-600 l/mm grating with the same slit, a setup that provides a maximum resolving power  $R \sim 1800$ , and a wavelength coverage 4500-6700Å.

The journal of the SOAR-Goodman observations is shown in Table 3, and the reduction of the optical spectra was performed using standard techniques through the use of the packages (beside others) ONEDSPEC, TWODSPEC and APEXTRACT within IRAF. The one-dimensional spectra of the science targets were extracted from the two dimensional frames by summing pixels in the data range and subtracting off the background value for each column, with the background for each column being measured as the median of non-target pixels for each column. Cosmic rays and other anomalous signal detection were suppressed from each of the extracted spectra, by removing pixels that deviate  $5\sigma$  of the mean within a 100 pixel wide box that steps through the spectrum. The bad pixels were replaced through a linear interpolation of the removed data range, and the wavelength calibration was performed using Hg(Ar) + Ne lamp spectra. As was made in the case of the NIR spectroscopic observations, the final optical spectra were also normalized through the fitting of the continuum emission in the associated wavelength range.

## 4. Results and Discussion

In Figures 2 and 3, we show the OSIRIS and Goodman normalized spectra of the sources in Table 2, with the exception of RFS10 for which we only have Goodman optical spectrum. The main NIR and optical spectral features are labeled by numbers, with the corresponding transitions being presented on the caption of the figures. As a complement, we also include there the NIR and optical spectra of HD93129A, the prototype of the O2If\* class, and until recently the unique known Galactic exemplar of this extreme O-type star with blue optical spectra published.

### 4.1. Spectral types

#### 4.1.1. *Three new Galactic exemplars of the OIf\*/WN intermediate type confirmed*

The intermediate spectral type OIf\*/WN was introduced about three decades ago by Walborn (1982) to classify the emission line star Sk-67 22 in the LMC, which shows spectral features between those of HD93129A (O2If\*) and WR20b (WN6ha). The OIf\*/WN type

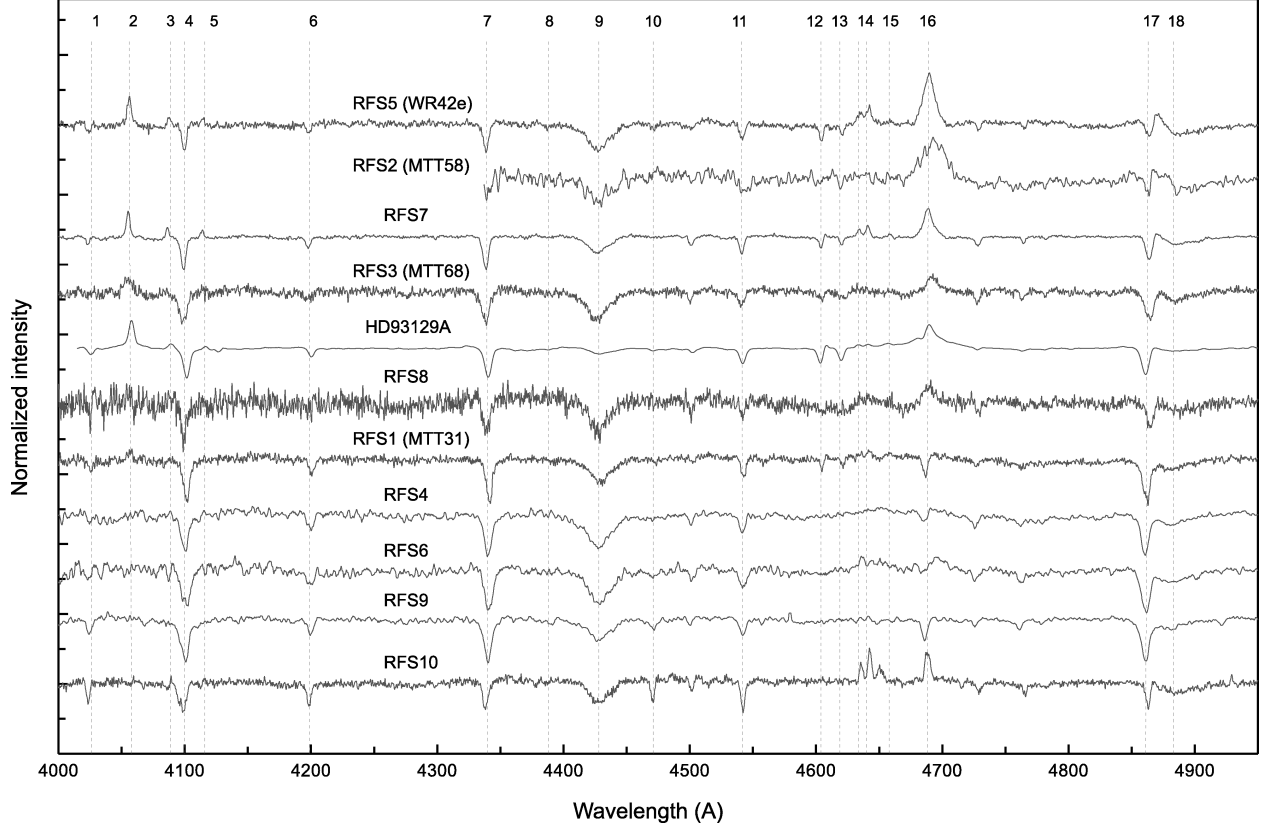


Fig. 3.— Goodman spectra of sources in Table 2. The main line features are indicated as follow (Walborn et al. 2002): (1) He I+II  $\lambda$ 4026, (2) N V  $\lambda$ 4058, (3) Si IV  $\lambda$ 4089, (4) H $\delta$ , (5) Si IV  $\lambda$ 4116, (6) He II  $\lambda$ 4200, (7) H $\gamma$ , (8) He I  $\lambda$ 4387, (9) DIB  $\lambda$ 4429, (10) He I  $\lambda$ 4471, (11) He II  $\lambda$ 4541, (12-13) N V  $\lambda\lambda$ 4604-4620, (14) N III  $\lambda\lambda$ 4634-4642, (15) C IV  $\lambda$ 4658, (16) He II  $\lambda$ 4686, (17) H $\beta$   $\lambda$ 4861, (18) DIB  $\lambda$ 4882.

can be separate from the OIf\* and WNH types by the P-Cygni morphology of the optical  $H\beta$  line since it is seen uniquely in absorption for O stars (including OIf\* stars) and purely in emission for WN stars (Crowther and Walborn 2011). From our NIR survey we identified three new Galactic exemplars of this class, RFS2 (MTT58), RFS5 (WR42e) and RFS7. As can be seen in Figure 2, their NIR spectrograms are characterized by the presence of strong  $Pa\beta$ ,  $Br\gamma$  and He II emission lines. On the other hand, from the optical spectra shown in Figure 3 we notice that they all (but RFS2 whose optical spectrum did not cover this wavelength range) present strong N IV  $\lambda 4058$  lines in emission, with all three also having powerful He II  $\lambda 4686$  emission lines, as well as  $H\beta$  lines showing P-Cygni profiles. Individual comments on the three new OIf\*/WN Galactic stars are given as follow:

**RFS5** As can be seen in Figure 3, RFS5 has the N IV  $\lambda 4058$  line intensity similar to those of the N III  $\lambda\lambda 4604-4620$  lines, and taking into account the He II  $\lambda 4686$  line purely in emission an O3If\* supergiant type is assigned. Based on the observed  $H\beta$  P-Cygni line profile, and following the criteria presented by Crowther & Walborn (2011), we are now able to refine the classification of this source by assigning it the O3If\*/WN6 type.

**RFS2** From the RFS2’s spectrograms shown in Figures 2 and 3, we can see that they resemble well those of RFS5. The P-Cygni profile in the  $H\beta$  line is also evident, confirming the previous classification based on NIR data made by Roman-Lopes (2013a), who classified it as a star of the OIf\*/WN (O2If\*/WN6) intermediate type. From the new optical data, it is now possible to improve this classification. Indeed, from the comparison of the strength of the N III  $\lambda\lambda 4604-4620$  lines of both stars, which are much weaker in the RFS2’s spectrogram than those seen in RFS5, we assign an O2If\*/WN5 spectral type to this star.

**RFS7** From Figure 2, we can see that RFS7 presents NIR spectral features similar to those seen in the spectrograms of RFS3. Indeed, the intensity (and morphology) of the  $Pa\beta$  and  $Br\gamma$  lines are quite similar. However, one also can notice that the He II  $\lambda 21890$  line appears much stronger in the K-band spectrum of RFS7, a characteristic also noticeable in the K-band spectra of RFS2 and RFS5, which combined with the  $Pa\beta$  broad emission line morphology, may be useful as complementary criteria when discriminating between the two types using solely NIR spectrograms. In this sense, the P-Cygni profile seen in the RFS7’s  $H\beta$  line indicates that this star is a new Galactic exemplar of the OIf\*/WN type. As a comment on this, the DIB seen at  $\lambda 4882$  appears relatively weak when compared with those present in the RFS5, RFS2 and RFS3 optical spectrograms. Curiously, the other strong DIB observed at  $\lambda 4429$  are all more or less of the same intensity, which might indicate that

its P-Cygni profile should seem stronger than the one observed. Accordingly to this, the observed line profile would be the result of the combination of two features: a relatively intense  $H\beta$  P-Cygni profile suppressed by a strong and broad DIB absorption line at  $\lambda 4882$ . Finally, the N IV  $\lambda 4058$  emission line stronger than the N III  $\lambda\lambda 4604-4620$  lines, indicates an intermediate type between O2If\*-O3If\* (Crowther & Walborn 2011), so we classify RFS7 as a O2.5If\*/WN6 star.

#### 4.1.2. RFS1 - The first Galactic exemplar of the O2V class identified to date

The NIR spectra of RFS1 (MTT31 - presented in Figure 2), are characterized by the presence of weak  $Pa\beta$ , and  $Br\gamma$  hydrogen recombination lines, which have peculiar absorption+emission profiles (probably indicative of presence of an intense stellar wind), similar to the one observed in the K-band spectrum of Cyg OB2 #7 (Hanson et al. 2006). Also, from a careful inspection of the  $\lambda\lambda 20600-21200$  spectral range one may see the existence of the C IV  $\lambda 20802$  line in absorption, together with the N V  $\lambda 21000$  line in emission, features normally only seen in K-band spectrograms of stars as early as HD64568 (O3 v((f))) and Cyg OB2 #7 (O3If\*). Moving to the H-band, we notice that the He I  $\lambda 17007$  line is absent in the RFS1's spectrum. However, it does show a strong He II  $\lambda 16930$  line in absorption, as well as the He II  $\lambda 21890$  in the K-band, indicating that RFS1 is a very hot star probably earlier than O3.

In Figure 3 it is shown the Goodman blue-optical spectrum of RFS1, and in order to allow a better analysis of it, in Figure 4 it is presented its individual spectrum in a more detailed and useful way. In particular, the weak lines close to the He II  $\lambda 4686$  line are better seen in this version of the spectrum. The N IV  $\lambda 4058$  line is seen in emission, and the strong He II absorption line at  $4200\text{\AA}$ , confirms the impression from our above discussion, e.g. that RFS1 is a very hot O-type star. In fact, the N IV  $\lambda 4058$ , and N III  $\lambda\lambda 4634-4642$  emission lines give strong support to this idea. Finally, the C IV  $\lambda 4658$  line clearly detected in emission led us to classify RFS1 as a new O2v star (Walborn et al. 2002). Indeed, based on a careful inspection of the blue-optical spectrum of BI 253 (the prototype of the O2v class (Walborn et al. 2002)) shown in figure 12 (a) of Massey et al. (2005), we can see that the RFS1 blue-optical spectrum is a nearly clone of it, which makes this star the first know Galactic exemplar of the O2v type (Sota et al. 2014).

On the other hand, the detection of what probably is a very weak He I  $\lambda 4471$  absorption line may suggests the presence of a later O-type companion. From a search in the literature, we found that RFS1 has an associated X-ray point source at only  $0.16''$  from its coordinates, catalogued as CXOU111506.69-611633.4 (Townesley et al. 2014). However, the observed X-

ray to bolometric luminosity ratio ( $\sim 3 \times 10^{-8}$ ) is found to be compatible with what is expected in case of a single star ( $L_X/L_\odot \sim 10^{-7}$ ). Further photometric and spectroscopic monitoring studies are necessary in order to test this assumption.

#### 4.1.3. *RFS3 confirmed as a new Galactic O2If\* star*

RFS3 (MTT68) was first catalogued as a probable member of NGC 3603 by Melnick, Tapia, & Terlevich (1989), and discovered to be a strong Chandra point source by Moffat et al. (2002), who performed an extensive X-ray to radio study of the  $3.6' \times 3.6'$  field centered on NGC 3603. Later, based on J-, H- and K-band SOAR-OSIRIS spectra it was classified as a O2If\* star by Roman-Lopes (2013a), who found its NIR spectra very similar to those of HD93129A, the template of the class (Walborn et al. 2002) and at that time, the only Galactic O2If\* previously known. Based on our new Goodman blue-optical spectra of RFS3 (shown in Figure 3), we may now confirm that this object is indeed a highly reddened O2If\* star, as indicate the strong diffuse interstellar bands (DIBs) seen at  $\sim 4430\text{\AA}$ , and  $4480\text{\AA}$ . As previously noticed by Roman-Lopes (2013a) in the NIR, the RFS3 optical spectrum also looks pretty similar to that of HD93129A, as indicate the intense N IV  $\lambda 4058$  emission line much stronger than the N III emission line pair at  $\lambda\lambda 4634\text{--}4642$ , which combined with the strong He II  $\lambda 4686$  emission line (Crowther & Walborn 2011), confirms its O2If\* nature. On the other hand, from a careful inspection of the NIR emission line features seen in the spectra of both stars (e.g. the Pa $\beta$  and the N III  $\lambda 21150$  lines), we can see that the observed emission lines appear broader in the RFS3 NIR spectrograms, a characteristic that is also quite evident in the N IV  $\lambda 4058$  optical line, which may suggest the existence of a secondary companion of RFS3, which in this case should also be another extreme early-type star.

#### 4.1.4. *New Early- and Mid-O Galactic supergiants*

Besides the O2If\* and OIf\*/WN stars discussed above, there are two other sources in Table 2 (RFS8 and RFS10) that show the He II  $\lambda 4686$  line in emission. Unfortunately, due to a problem during the acquisition process, the NIR spectra of RFS10 resulted not useful for spectral analyses, so in its case our main conclusions only rely on optical data. In what follows, we discuss in some detail the results obtained for this two objects.

**RFS8** The NIR spectrograms of the RFS8 source (shown in Figure 2), are dominated by emission line features associated to the Pa $\beta$ , Br $\gamma$ , Br10, and Br11 hydrogen atomic

transitions, as well as by broad emission line profiles corresponding to the C IV  $\lambda\lambda 20690$ - $20802$  and N III  $\lambda 21160$  transitions. The morphology of the Pa $\beta$  emission line is quite similar (on both shape and intensity) to the one seen in the J-band spectrum of HD93129A, however, the Br $\gamma$  line profile is completely different. Also, the He II lines  $\lambda 16930$  and  $\lambda 21890$  appear in absorption, suggesting a later spectral type. The blue-optical spectrum for this source (shown in Figure 3) confirms this assumption. The intense emission feature associated to He II  $\lambda 4686$  indicates a supergiant status for this object. The N IV  $\lambda 4058$  emission line is less intense than those of the N III  $\lambda\lambda 4634$ - $4642$  pair, which combined with the N V  $\lambda\lambda 4604$ - $4620$  lines weaker than those seen in the HD93129A blue-optical spectrogram, indicate a spectral type later than O3. Finally, the absence of a He I  $\lambda 4471$  absorption line, suggests a spectral type probably no later than O4-O4.5 (Sota et al. 2011). Taking into account the points discussed above, and the criteria presented by Crowther & Walborn (2011), we assign an O3.5If\* spectral type to the RFS8 source.

**RFS10** As mentioned before, for this star we only have optical data, and its spectrogram is shown in Figure 3. It is a high S/N optical spectrum in which the He II  $\lambda 4686$  emission line denotes a supergiant class for this source. The absence of N V  $\lambda\lambda 4604$ - $4620$  lines associated to the presence of a strong He I  $\lambda 4471$  absorption line, indicate that this star is of spectral type later than O3.5-O4 (Sota et al. 2011). Also, from the library of optical spectra of O-stars of Sota et al. (2011), one can see that the relative intensity of the two N III  $\lambda\lambda 4634$ - $4642$  emission lines and the He I  $\lambda 4471$  and He II  $\lambda 4541$  absorption lines, make this spectrum pretty similar to that of HD 169582 the standard of the O6Ia type. We searched in the literature looking for X-ray sources associated to RFS10 founding a strong one in the XMM-Newton catalogue at only  $0.35''$  from RFS10's coordinates, identified as J111955.1-611603. Further photometric and spectroscopic studies are indicated for this source, as the detected X-ray emission could be due to the presence of a close binary companion.

#### 4.1.5. *early-O type stars*

The sources in this group are RFS4, RFS6 and RFS9, whose spectral features are typical of early and mid-O type stars. In the following, we discuss each object in detail.

**RFS4 (MTT71)** The J-, H-, K-band spectra of RFS4 (presented in Figure 2) are very similar to those of RFS1, with a small but remarkable difference: the presence of He I  $\lambda 17007$  absorption line, which however is less intense than the He II  $\lambda 16930$  line. This feature indicates that this source is also an early O-type star, and from a comparison with the H-band spectra

of HD46223 (O4v), HD66811 (O4 I), HD14947 (O5 If) and Cyg OB2 8c (O5 If) (Hanson et al. 2006), one may see that the H- and K-band features of RFS4 are compatible with those seen in O-type stars of spectral types O4-O5. On the other hand, the Goodman normalized spectrum of RFS4 (shown in Figure 3), does not show the He I  $\lambda 4471$  absorption line, so an early O-type status for this star is confirmed. Also, the absence of a N IV  $\lambda 4058$  line (in emission or absorption) indicates that this star is of spectral type not earlier than O4. Indeed, the optical spectrum of HD168076AB (O4III) is virtually a clone of the RFS4 Goodman spectrogram, including the incipient P-Cygni profile seen in its He II  $\lambda 4686$  line, allowing us to classify RFS4 as a new Galactic O4III star. As a final comment on this source, from a cross check with X-Ray catalogues in the literature, we found a point source (at only  $0.05''$  from it) catalogued as CXOU111521.31-611504.3 (Townsend et al. 2014). Indeed, RFS4 was first discovered as a strong X-ray point source by Moffat et al. (2002) who pointed that it could be due to colliding wind binary interaction, which may suggest the existence of an early O-type companion. Further studies are necessary in order to properly address this assumption.

**RFS6** The OSIRIS and Goodman spectra for this source look pretty similar to those of the RFS4 source. Indeed, the presence of strong He II  $\lambda\lambda 16930$ - $21890$  absorption lines, the weakness of He I  $\lambda 17007$  transition combined with the absence of the He I absorption line  $\lambda 21130$  give support to this idea. Also, taking into account the presence of strong C IV and N III  $\lambda\lambda 20800$ - $21160$  emission lines led us to the conclusion that this star is probably another exemplar of the early type O-star family. In support to that, the optical spectrogram shown in Figure 3 also looks pretty similar to that of RFS4, except for the He I  $\lambda 4471$  line which is clearly seen (weakly) in absorption, which is not uncommon for O4-5 stars like HD46223 (O4v), HD66811 (O4I), HD14947 (O5If) and Cyg OB2 8c (O5If) (Hanson et al. 2006).

**RFS9** The NIR spectrograms of the RFS9 source are shown in Figure 2. As can be seen there, its J-band spectrum presents a strong and broad Pa $\beta$  absorption line, a feature also noticed on the profiles of the H- and K-band Bracket lines. The He II lines at  $\lambda 16930$  and  $\lambda 21890$  are also seen in absorption, and there is no sign of the He I line at  $21113\text{\AA}$ , so a spectral type later than O6v is ruled out (Hanson et al. 2006). On the other hand, the He I absorption line  $\lambda 17007$  is stronger than the He II  $\lambda 16930$ , an indication that this star is possibly of a type later than O4. From the optical spectrogram of the RFS9 source, shown in Figure 3, we can see that the He II  $\lambda 4686$  line is seen purely in absorption, so a dwarf class is assigned. Based on the above discussion, we performed a careful examination of O4v-O5v optical spectra presented in the literature, concluding that our Goodman spectrum of the source RFS9 looks pretty similar to those of HD15629 (O4.5v), HD46150 (O5v)



and HD93204 (O5v), presented in Sota et al. (2011), and that of source #108 (O5.5v) of Melena et al. (2008). An interesting spectral characteristic that kept our attention is the He II  $\lambda\lambda 4686$  absorption line stronger than any other He II lines present in the  $\lambda\lambda 4000$ -5000 wavelength range. Such O-type spectral feature is believed to be characteristic of the Vz class. It seems that the Of effect (established as a luminosity indicator in normal O-type spectra) is suppressed by the Vz effect, generating less emission than in normal class V spectra, which might indicate extreme stellar youth (Walborn et al. 2014).

A natural question that arises from this result is, how such an extremely young O-star could be found at such a large angular distance from the NGC3603 cluster center? A possible answer is that RFS9 belongs to an independent star forming complex embedded in the main body of the NGC3603 complex. In an upcoming paper (Roman-Lopes et al. in preparation), we further discuss the issue on how so many of the sources in Table 2 could have arrived at their present location.

## 4.2. Interstellar extinction, absolute magnitudes, ages and masses

### 4.2.1. Interstellar extinction

The interstellar extinction law in the direction of NGC 3603 appears to be anomalous. This is not surprisingly as it is well known that very young HII regions in general show ratio of total to selective extinction values well above the canonical value  $R_V=3.1$  (Chini & Kruegel 1983; Chini & Wargau 1990). Pandey, Ogura & Sekiguchi (2000) performed an extensive UBVRI CCD photometric survey in the direction of the innermost region ( $2.08' \times 3.33'$  FOV) of the cluster, and from a variable extinction analysis of the sources with color excess in the range  $1.30 < E(B-V) < 1.75$ , they computed a mean value for the total to selective extinction ratio  $R_V=3.8 \pm 0.8$ . The large uncertainty on the mean reflects the large scatter on the individual derived values. Also, by following the method of Neckel & Chini (1981) they were able to obtain the intra-cluster total to selective extinction ratio value  $R_V=4.1 \pm 0.2$ .

In Table 4 besides the spectral types and effective temperatures, we present the (B-V) colors for each star in our sample, together with the associated optical to NIR color excesses  $E(B-V)$ ,  $E(J-V)$ ,  $E(H-V)$  and  $E(K-V)$ , which were derived using the intrinsic colors for the earliest O-stars given by Martins & Plez (2006). The values of the total to selective extinction ratio were then estimated using the equations A3-A6 of Fitzpatrick (1999), and by using  $R_V$  and  $E(B-V)$ , we computed the corresponding extinction parameter  $A_V$  for each

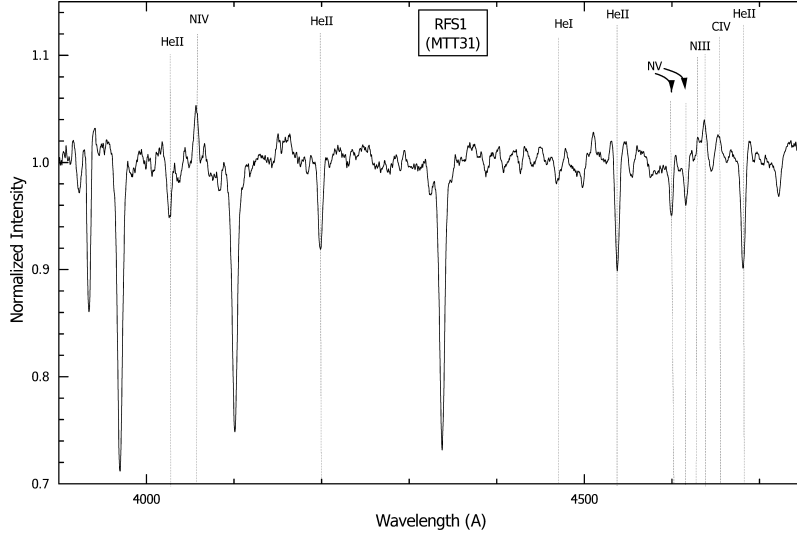


Fig. 4.— Goodman spectrum of RFS1 source. The main line features are indicated as follow (Walborn et al. 2002): (1) He I+II  $\lambda$ 4026, (2) N v  $\lambda$ 4058, (3) He II  $\lambda$ 4200, (4) He I  $\lambda$ 4471, (5) He II  $\lambda$ 4541, (6) N v  $\lambda\lambda$ 4604-4620, (7) N III  $\lambda\lambda$ 4634-4642 , (8) C IV  $\lambda$ 4658, (9) He II  $\lambda$ 4686

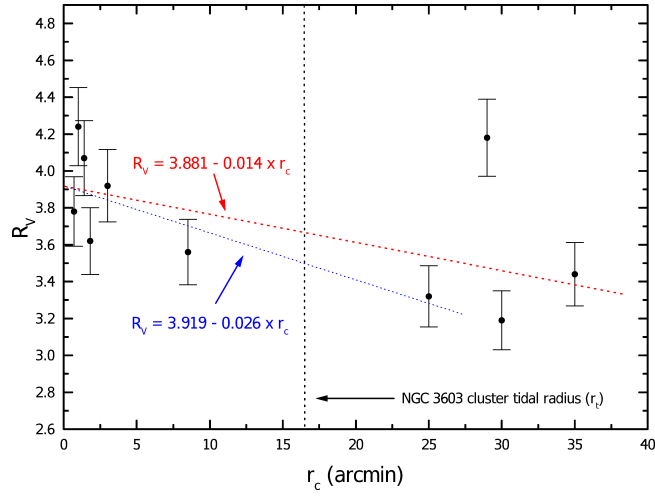


Fig. 5.—  $R_V$  as a function of the cluster center radius  $r_c$  for sources in Table 4. We can see that with the exception of RFS8, the associated  $R_V$  values decreases approximately linearly as a function of  $r_c$ . In the same plot we also present the results of linear fittings considering all sources in the sample, as well as those (six) presenting  $r_c$  values less than the NGC 3603 cluster tidal radius estimated by Sung & Bessell (2004).

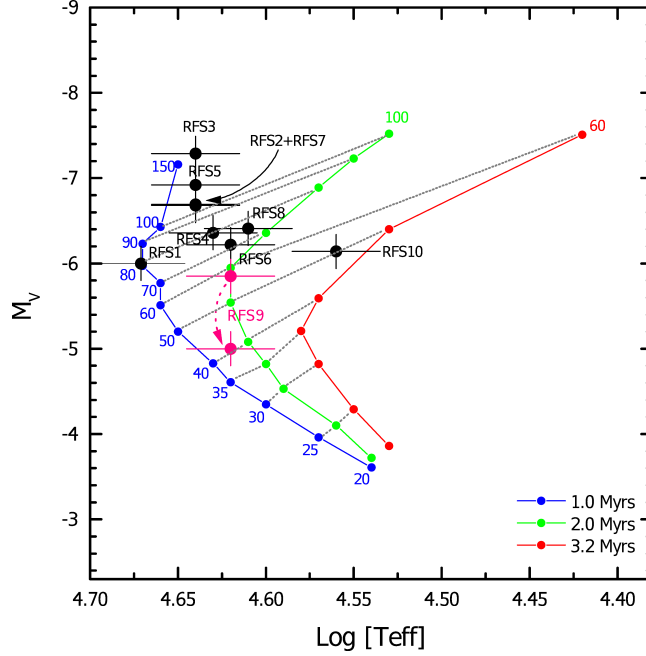


Fig. 6.— The  $M_V$  versus  $\text{Log } T$  (Teff) Hertzsprung-Russel diagram for sources in Table 4. The effective temperatures for the OI, OIII and OV classes were computed using Equation 2 presented in the work of Martins et al. (2005), while the values for the OIf\*/WN stars were estimated from the work of Crowther et al. (2010). For all sources we assumed an uncertainty of  $\pm 3000\text{K}$  on the quoted temperature values. We also present there the 1 Myr, 2 Myrs and 3.2 Myrs isochrons taken from the work of Bressan et al. (2012), for stars with initial masses in the range  $20\text{-}150M_{\odot}$  (solar metallicity  $Z=0.015$ ). RFS9 is represented considering single and binary systems comprised by two stars of same spectral type. In this sense, assuming a mean absolute visual magnitude  $M_V = -5.0$  for each component would result in a combined absolute magnitude  $M_V = -5.8$ , a value in line with the one derived by us (considering the associated uncertainties) using the distance modulus equation, equivalent to a binary system comprised by two stars of  $40 M_{\odot}$  each (see text in Section 4.2.2).

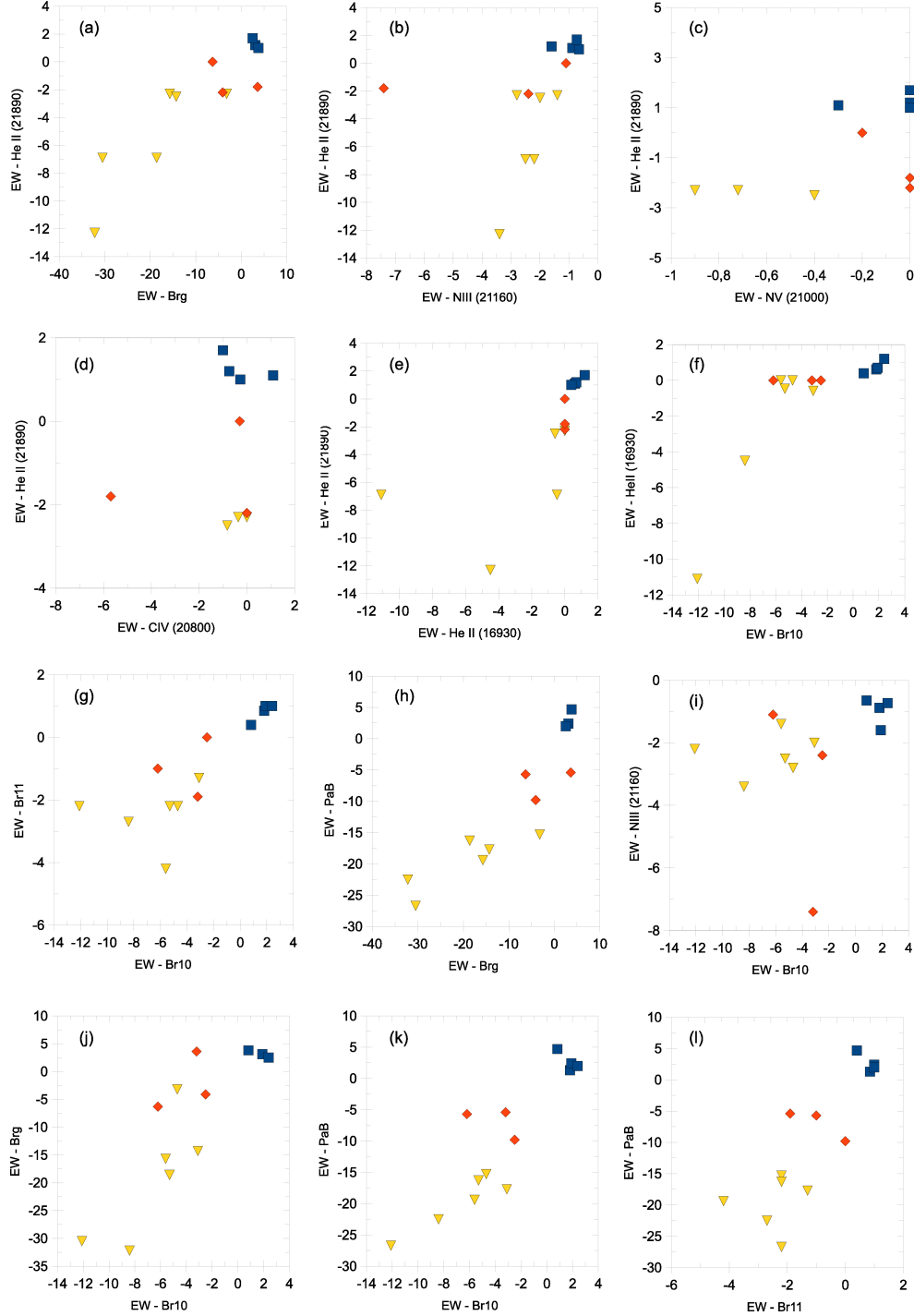


Fig. 7.— Observed values of EWs ( $\text{\AA}$ ) for O (squares), OIf\* (diamonds) and OIf\*/WN type (triangles) stars in Table 5. As can be noticed from panels 7(e) to 7(l), the use of H- and J-bands spectral line measurements can also provide a good separation of the distinct types. In fact, the combination of the Br10, Br11 and Pa $\beta$  hydrogen line measurements is particularly useful when separating the transitional OIf\*/WN stars from the OIf\* ones. In this sense, good results are achieved using Pa $\beta$  line measurements combined with the H-band hydrogen transitions.

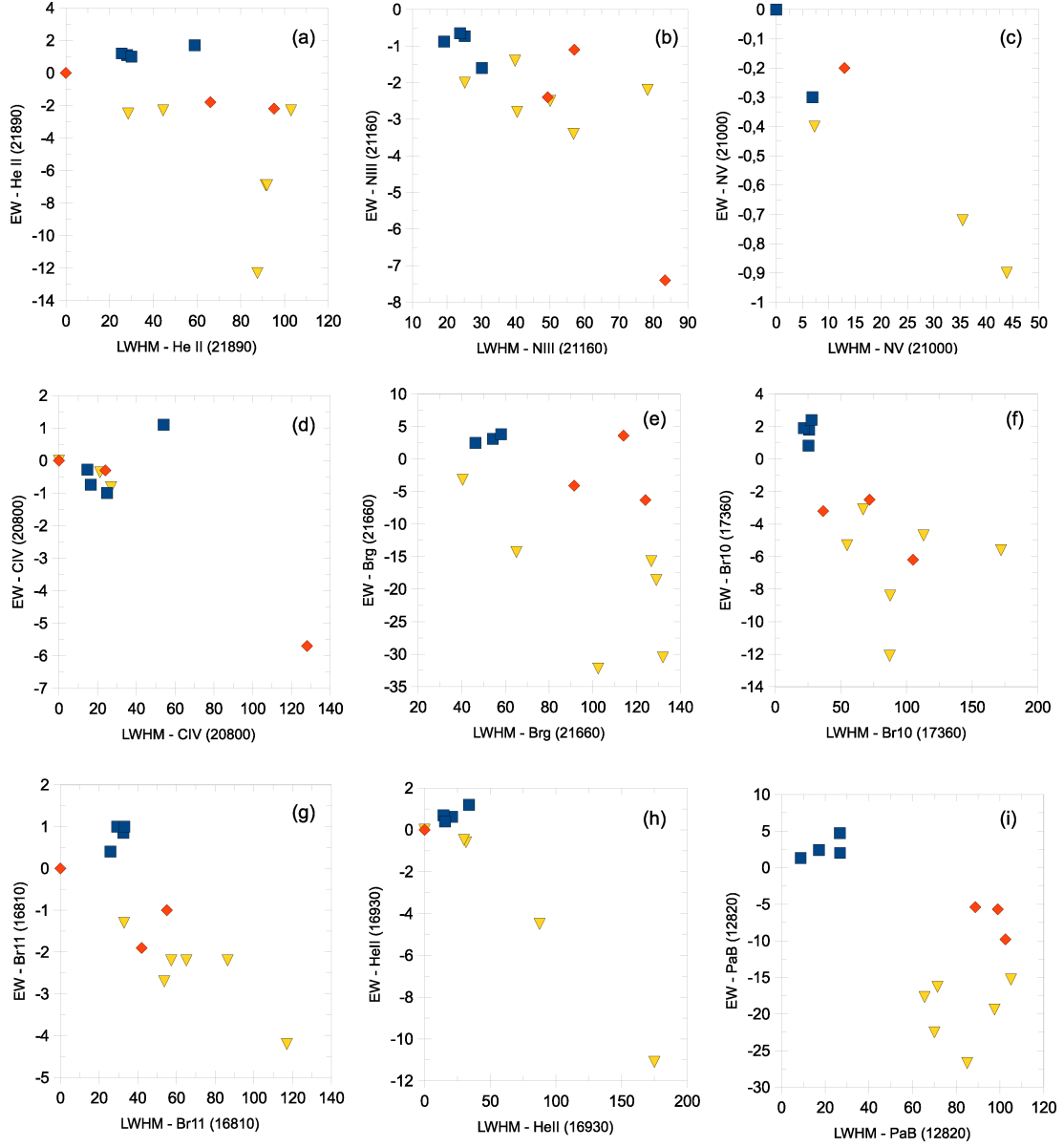


Fig. 8.— Observed values of  $EW \times LWHM$  (Å) for O (squares), OIf\* (diamonds) and OIf\*/WN type (triangles) stars in Table 5.

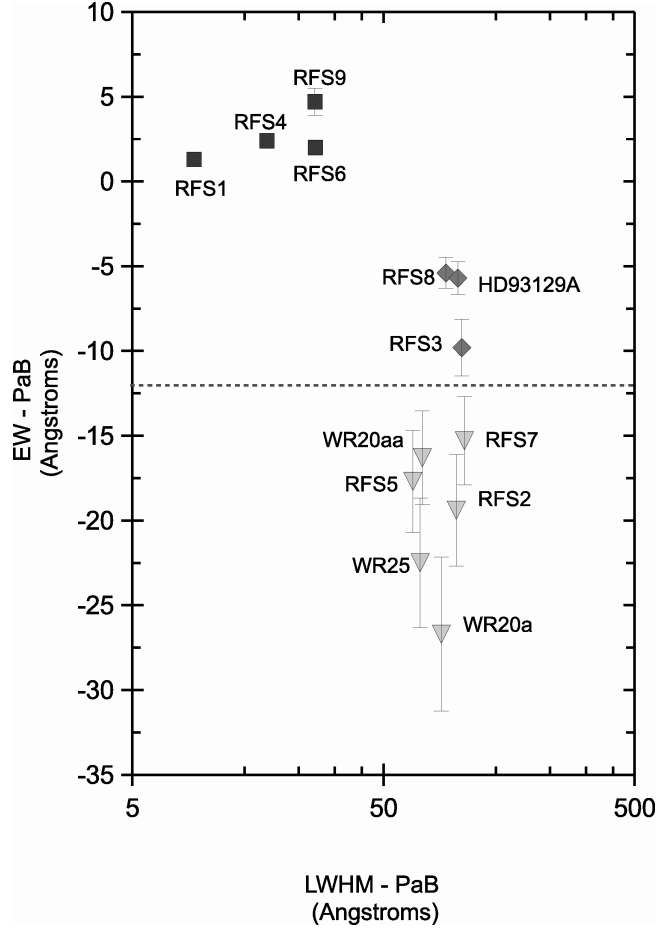


Fig. 9.—  $EW \times LWHM$   $Pa\beta$  values for O (squares), OIf\* (diamonds) and OIf\*/WN type (triangles) stars in Table 5. The results for the  $Pa\beta$  emission line indicate that the transition boundary between OIf\* and OIf\*/WN stars occurs for  $EW(Pa\beta) \sim 12\text{\AA}$ , always for spectral lines showing  $LWHM(Pa\beta)$  values above  $\sim 60\text{\AA}$ .

Table 4. Spectral types, absolute magnitudes and extinction law parameters obtained for sources in Table 2. (1) ID, (2-6) (B-V) colors and associated optical to NIR color excesses. The color-excesses were calculated using the corresponding  $(B-V)_0$ ,  $(J-V)_0$ ,  $(H-V)_0$  and  $(K-V)_0$  intrinsic colors taken from Martins & Plez (2006). (7) The total to selective extinction ratio  $R_V$  values were derived using the equations A3 to A6 of Fitzpatrick (1999). (8) Visual extinction computed from  $E(B-V)$  and  $R_V$ . (9) Absolute visual magnitudes  $M_V$  obtained using  $A_V$  plus the visual magnitudes for each source in Table 2, applied into the distance modulus equation for an heliocentric distance of  $7.6 \pm 0.35$  kpc (Crowther et al. 2010). (10-12) The same for the  $M_J$ ,  $M_H$  and  $M_K$  absolute magnitudes, using the V-J, V-H and V-K color values taken from Martins & Plez (2006). (13-15)  $A_J$ ,  $A_H$  and  $A_K$  extinction values derived using the J-, H- and K-band magnitudes from Table 2, together with the associated  $M_J$ ,  $M_H$  and  $M_K$  values applied into the distance modulus equation.

Source	SpType	Log Teff	(B-V)	E(B-V)	E(J-V)	E(H-V)	E(K-V)	$R_V$	$A_V$	$M_V$	$M_J$	$M_H$	$M_K$	$A_J$	$A_H$	$A_K$
RFS1	O2 V	4.67	1.22	1.50	-4.07	-4.69	-5.09	3.78	5.67	-6.00	-5.33	-5.21	-5.12	1.60	0.98	0.58
RFS2	O2 If*/WN5	4.64	1.38	1.66	-4.96	-5.87	-6.40	4.24	7.04	-6.68	-6.01	-5.89	-5.80	2.08	1.17	0.64
RFS3	O2 If*	4.64	1.59	1.87	-5.41	-6.34	-6.86	4.07	7.61	-7.29	-6.62	-6.50	-6.41	2.20	1.27	0.75
RFS4	O4 III	4.63	1.57	1.85	-4.81	-5.54	-6.02	3.62	6.70	-6.36	-5.69	-5.57	-5.48	1.89	1.16	0.68
RFS5	O3 If*/WN6	4.64	1.52	1.80	-5.02	-5.85	-6.37	3.92	7.05	-6.92	-6.25	-6.13	-6.04	2.03	1.20	0.68
RFS6	O4.5 V	4.62	1.50	1.78	-4.55	-5.25	-5.67	3.56	6.33	-6.22	-5.55	-5.43	-5.34	1.78	1.08	0.66
RFS7	O2.5 If*/WN6	4.64	1.28	1.56	-3.71	-4.29	-4.65	3.32	5.18	-6.69	-6.02	-5.90	-5.81	1.47	0.89	0.53
RFS8	O 3.5If*	4.61	1.32	1.60	-4.74	-5.55	-6.08	4.18	6.69	-6.41	-5.74	-5.62	-5.63	1.95	1.14	0.61
RFS9	O5 Vz	4.61	1.36	1.64	-3.74	-4.35	-4.67	3.19	5.22	-5.85	-5.18	-5.06	-4.97	1.48	0.87	0.55
RFS10	O6 Ia	4.56	1.35	1.63	-3.99	-4.62	-5.08	3.44	5.60	-6.14	-5.47	-5.35	-5.26	1.61	0.98	0.52

star in Table 2. From the  $R_V$  values in Table 4, we can see that for most of the stars in our sample the associated interstellar law is in agreement with the previous study of Pandey, Ogura & Sekiguchi (2000), with  $R_V$  ranging from 3.19 for RFS9 to 4.24 in case of RFS2, with mean value and standard deviation of the mean  $R_V=3.73\pm0.35$ . As in the previous studies, the relatively large error value on the mean probably reflects the moderate scatter on the computed ratio of total to selective extinction in the direction of NGC 3603, which in turn is probably produced by the variations on the dust and gas column densities, and perhaps on differences on dust composition and grain sizes.

In Figure 5, we plot the parameter  $R_V$  as a function of the cluster center distance  $r_c$  for sources in Table 4. We can see that with the exception of RFS8, the associated  $R_V$  values decreases as a function of  $r_c$ . In the same plot we also present the results of linear fittings considering all sources in the sample, as well as only those (six) presenting  $r_c$  values less than the NGC 3603 cluster tidal radius estimated by Sung & Bessell (2004). The resulting linear equations correlating  $R_V$  and  $r_c$  are  $R_V = 3.881 - 0.014r_c$  and  $R_V = 3.919 - 0.026r_c$ , for the entire sample and only for those sources inside the NGC 3603 tidal radius area, respectively. The values of  $R_V$  computed from our fittings limited to the radial cluster center distance of 2 arcmin are  $R_V = 3.85$  and  $R_V = 3.87$ , respectively, in good agreement with the result obtained by Pandey, Ogura & Sekiguchi (2000). Finally, from the extinction parameters presented in Table 4, we computed mean values and uncertainties (errors on the mean) of the ratios  $A_\lambda/A_V$  for the J-, H- and  $K_S$ -bands obtaining  $A_J/A_V = 0.286\pm0.004$ ,  $A_H/A_V = 0.170\pm0.003$  and  $A_{K_S}/A_V = 0.098\pm0.005$ .

#### 4.2.2. Absolute magnitudes, ages and masses

The absolute magnitudes for sources in Table 4 were derived using the observed magnitudes and associated extinction values applied into the distance modulus equation, adopting an heliocentric distance of  $7.6\pm0.35$  kpc (Crowther et al. 2010). Also, the respective  $M_J$ ,  $M_H$  and  $M_K$  absolute magnitudes were calculated using the  $(V-J)_0$ ,  $(V-H)_0$  and  $(V-K)_0$  intrinsic colors for early-O stars taken from Martins & Plez (2006). In Figure 6, we present the  $M_V$  versus Log T (Teff) Hertzsprung-Russel (H-R) diagram for sources in Table 4. The effective temperatures for the OI, OIII and OV classes were obtained using Equation 2 presented in the work of Martins et al. (2005), while the values for the OIf\*/WN stars were estimated from the work of Crowther et al. (2010). For all sources we assumed an uncertainty of  $\pm3000K$  on the quoted values. We also present there the 1 Myr, 2 Myrs and 3.2



Myrs isochrons<sup>2</sup> taken from the work of Bressan et al. (2012), for stars with initial masses in the range 20-150 $M_{\odot}$ (solar metallicity  $Z=0.015$ ).

From this diagram we can see that the youngest sources are RFS1, RFS2, RFS3, RFS5 and RFS7 with probable ages of about 1 Myrs. The new O2If\* star (RFS3) with initial mass above 150  $M_{\odot}$ , appears as the most massive and luminous object of our sample. This is not surprising as O2If\* stars are known to belong to the most massive and luminous type of O-stars in the local universe. For example, HD93129A the most massive and luminous O-star previously known in the Galaxy has an absolute visual magnitude  $M_V=-6.6$  (Simon et al. 1983) and estimated initial mass of  $130\pm15 M_{\odot}$  (Taresch et al. 1997). On the other hand, in the LMC we have the extreme case of Mk42, an O2If\* star presenting absolute visual magnitude  $M_V=-7.4$ , and initial mass of 189  $M_{\odot}$  (Bestenlehner et al. 2014).

Accordingly with the isochrons shown in Figure 6, all three new Galactic OIf\*/WN stars had initial masses well above 100  $M_{\odot}$ , with RFS5 (O3If\*/WN6) being a bit more massive than RFS2 and RFS7. Placed in the same star forming complex, NGC3603-C has the same spectral type (O3If\*/WN6), with  $M_V=-7.2$  and estimate initial mass in the range 123-154  $M_{\odot}$  (Crowther et al. 2010). Taking into account the evolutionary models and the RFS5's position in the H-R diagram of Figure 5, we can conclude that for an estimated age of 1 Myr, RFS5 should have initial and current masses of 135  $M_{\odot}$  and 123  $M_{\odot}$ , respectively, a result in line with those obtained by Crowther et al. (2010) in their analyses of NGC3603-C. Besides the three new OIf\*/WN stars, another very young star in our sample is RFS1. From its position in the H-R diagram of Figure 6, we can see that it is an O2v star with probable initial and current masses of 80  $M_{\odot}$  and 76  $M_{\odot}$ , respectively. As the only Galactic star of its class known to date, RFS1 has an absolute magnitude  $M_V=-6.0$ , corresponding to a luminosity similar to other O2v stars found in the LMC, like VFTS 621 (O2v and VFTS 512 (O2v-III) both presenting visual absolute magnitudes  $M_V=-6.1$  (Bestenlehner et al. 2014).

A second group of sources slightly older with ages ranging from 1.5-2.0 Myrs, is comprised by RFS4 (O4III), RFS6 (O4.5III), RFS8 (O3.5If\*) and RFS9 (O5Vz). From their associated absolute visual magnitudes (Table 4) we can see that they appear also as very luminous sources, and based on the comparison of such values with those from other stars of similar spectral types, we conclude that our results are in line with those found in the literature, with the exception of RFS9, which appears more luminous than what is expected from the comparison with other LMC and Galactic O5vz stars. We will discuss more about this source later.

The absolute visual magnitudes of RFS4 and RFS6 are quite consistent with the values

---

<sup>2</sup><http://stev.oapd.inaf.it/cgi-bin/cmd>

for stars of similar spectral types found in the LMC, as for example VFTS 422 (O4III) -  $M_V = -5.8$ , VFTS 603 (O4III) -  $M_V = -6.3$ , and VFTS 608 (O4III) -  $M_V = -6.0$ . On the other hand, in the Milk Way we have the cases of HD 168076 (O4III) with absolute visual magnitude  $M_V = -5.9$  (Sana, Gosset & Evans 2009), HD 93250 AB (O4III) presenting  $M_V = -6.2$  with an estimated stellar mass of  $83 M_\odot$  (Repolust, Puls & Herrero 2004), as well as in the innermost part of NGC 3603, the source #38 of Melena et al. (2008) (O4III) with  $M_V = -6.0$ .

The case of RFS8 (O3.5If\*) is quite interesting. Indeed, it is located well to the south of the complex, in apparent isolation at the large radial angular center distance of  $29'$ , or equivalently, at a projected linear distance of about 62 pc considering the quoted NGC 3603 heliocentric distance of 7.6 kpc. Based on its location in the H-R diagram of Figure 5 and accordingly with the stellar evolutionary models, RFS8 would have initial and current masses of  $77 M_\odot$  and  $70 M_\odot$ , respectively. Its derived absolute magnitude  $M_V = -6.4$  is similar to that of another O3.5If\* (Sh18) found in the NGC 3603's innermost region, with an absolute magnitude  $M_V = -6.3$  (Bestenlehner et al. 2011). The fact that a such high mass star is found isolated in the field naturally led us to speculate if it could have been expelled sometime in the past from the innermost parts of the complex. Looking for proper motion measurements for this star and based on a search on the PPMXL and XPM proper motion catalogues (Roeser, Demleitner & Schilbach 2010; Fedorov 2011), we found that RFS8 has proper motion parameters  $\text{pmRA} = -34.3 \pm 11.8$  mas/yr -  $\text{pmDE} = -53.2 \pm 11.8$  mas/yr and  $\text{pmRA} = -40.0 \pm 10.0$  mas/yr -  $\text{pmDE} = -58.6 \pm 10.0$  mas/yr, respectively, quite high for an object that is assumed to be placed at the same heliocentric distance of NGC 3603. Indeed, considering a distance of  $7.6 \pm 0.35$  kpc would results in a projected linear velocity of about 240 km/s! Despite such a high velocity for a very high mass star at first might seen unlikely, Gvaramadze & Gualandris (2011) showed from their study on the dynamical ejection scenario of massive runaway stars that such a high mass runaway star could actually exist. Indeed, they argue that the most effective process generating this kind of high velocity star is that produced by a close fly-by dynamical encounter between a single massive star with a very massive hard binary system. For example, in the case of a NGC3603-A1-like binary system ( $M_1 = 120 M_\odot + M_2 = 90 M_\odot$ ), in a few percent of the cases a  $60\text{-}80 M_\odot M_3$  fly-by star would acquire a peculiar velocity as high as 250 km/s. In this sense, further proper motion measurements like those to be provided by the Gaia space astrometry mission, are necessary to give (or not) additional support to this idea.

From RFS9's location in the HR diagram of Figure 5, we can see that its derived absolute magnitude ( $M_V = -5.85$ ) is not consistent with the absolute visual magnitudes for single stars of the O5vz type in the LMC, like for example VFTS 385 ( $M_V = -5.2$ ,  $\log(\text{Teff}) = 4.63$ ), VFTS 511 ( $M_V = -4.9$ ,  $\log(\text{Teff}) = 4.64$ ), and VFTS 581 ( $M_V = -5.0$ ,  $\log(\text{Teff}) = 4.60$ ) (Sabín-Sanjulián et al. 2014). A possible explanation for this discrepancy can be

obtained if we consider the case in which RFS9 is a binary system comprised by two stars of same spectral type. In this sense, assuming a mean absolute visual magnitude  $M_V = -5.0$  for each component would result in a combined absolute magnitude  $M_V = -5.8$ , a value in line with the one derived by us (considering the associated uncertainties) using the distance modulus equation. In this case, from Figure 5 we can see that RFS9 would be a binary system comprised by two stars of  $40 M_\odot$  each.

With an estimated age of about 3 Myrs (accordingly with the isochrons of Bressan et al. (2012)), RFS10 appears as the oldest star in our sample with initial and current masses of  $45\text{--}55 M_\odot$  and  $40\text{--}50 M_\odot$ , respectively. Its derived absolute visual magnitude  $M_V = -6.14$  and spectroscopic mass of  $45\text{--}55 M_\odot$  agree with the corresponding values obtained for Galactic O5-O6Ia stars ( $M_V = -6.1$ ) (Wegner 2005), as well as with the values of stars of similar spectral type and luminosity class in the LMC, like VFTS 151 (O6.5II(f)p -  $M_V = -6.4$ ,  $M = 79 M_\odot$ ), VFTS 208 (O6 (n)fp -  $M_V = -5.8$ ,  $M = 53 M_\odot$ ) and VFTS 440 (O6-O6.5II(f) -  $M_V = -6.2$ ,  $M = 76 M_\odot$ ).

#### 4.3. Identifying the OIf\*/WN type solely from near-IR spectrograms

With the usage of new efficient detectors and large ground-based telescopes, the near-IR window has become available for spectral typing (Hanson, Conti & Rieke (1996); Hanson et al. (2006); Crowther & Walborn (2011), and references therein). This is particularly important when dealing with highly obscured and distant early-type stars. However, despite the observational progress made during the last years, the number of known Galactic OIf\*/WN stars with some study in both, optical and near-IR domains is relatively small. Considering that the majority (if not all) of the remaining members of the OIf\*/WN Galactic stellar population probably is going to be discovered (and properly studied), mainly from the use of NIR spectroscopic facilities, one important question (already made by Crowther & Walborn (2011)) is, can we safely distinguish between the OIf\* and OIf/WN types using only near-IR spectroscopy? In order to contribute to address this question, in the next we will make use of the NIR spectral line measurements taken from our new set of Galactic O, OIf\* and OIf\*/WN stars, which were spectroscopically classified using the data taken with OSIRIS and Goodman at SOAR.

In Tables 5 and 6 we present the equivalent width (EW) and line width (LW) measurements made from the observed NIR and optical lines. As a complement we also present in Table 5 the EW and LW measurements of relevant NIR lines, obtained from a set of unpublished J-, H- and K-band OSIRIS spectra of WR20a (O3If\*WN6+O3If\*/WN6), WR20aa (O2If\*/WN5) and WR25 (O2.5If\*/WN6+O) (Rosslowe & Crowther 2015), taken during pre-

vious nights with SOAR. From the associated values, we constructed EW and EW $\times$ LWHM comparative diagrams shown in Figure 7 and Figure 8, respectively, and based on them, one can see that the normal O-type stars (represented by the blue squares) in general are seen well separated from the OIf\* and OIf\*/WN stars. This is particularly true even when considering spectral lines seen in emission in all NIR spectrograms, like for example the N III  $\lambda\lambda$ 21160 transition (panel 7(b)). On the other hand, the separation of the normal O-type stars from the OIf\* and OIf\*/WN groups is clearly seen in all remaining panels of Figure 7.

In the particular case of using only the K-band to separate normal O-type stars from the OIf\* and OIf\*/WN types, the best comparative diagram to be used is the one presenting the He II  $\times$  Br $\gamma$  EW line measurements, as seen in panel 7(a). In fact, in this case it is possible not only to identify the locus of normal O-type stars, but also to separate the majority of the OIf\*/WN type stars from the OIf\* group. This is particularly evident for those OIf\*/WN stars presenting He II  $\lambda\lambda$ 21890 and Br $\gamma$  line width values satisfying simultaneously the condition  $\text{EW}(\text{He II}) < -2\text{\AA}$ , and  $\text{EW}(\text{Br}\gamma) < -12.5\text{\AA}$ , which correspond to a combined width  $W_\lambda(\text{Br}\gamma + \text{He II}) \sim 15\text{\AA}$ , about half of the value suggested by Crowther & Walborn (2011) for the criterium defining the boundary between OIf\* and OIf\*/WN stars. On the other hand, as can be noticed from panels 7(e) to 7(l), the use of H- and J-bands spectral line measurements can also provide a good separation of the distinct types. In fact, the combination of the Br10, Br11 and Pa $\beta$  hydrogen line measurements is particularly useful when separating the transitional OIf\*/WN stars from the OIf\* ones. In this sense, good results are achieved using Pa $\beta$  line measurements combined with the H-band hydrogen transitions, as can be seen in panels 7(k) for EW (Pa $\beta$ )  $\times$  EW (Br10) and 7(l) for EW (Pa $\beta$ )  $\times$  EW (Br11).

From such diagrams one may conclude that the approximate values defining the boundaries between OIf\* and OIf\*/WN stars are those corresponding to combined equivalent widths  $\text{EW}_\lambda(\text{Br}\gamma + \text{pa}\beta) > 18\text{\AA}$  (panel 7(h)),  $\text{EW}_\lambda(\text{Br10} + \text{pa}\beta) > 20\text{\AA}$  (panel 7(k)), and  $\text{EW}_\lambda(\text{Br11} + \text{pa}\beta) > 16\text{\AA}$  (panel 7(l)). Finally, regarding approximate boundaries between subtypes analogous to the criterium using the He II  $\lambda$ 4686 in the optical window (Crowther & Walborn 2011), the results for the Pa $\beta$  emission line are shown in Figure 9. There it is clearly seen that the transition boundary between OIf\* and OIf\*/WN stars occurs for  $\text{EW}(\text{Pa}\beta) \sim 12\text{\AA}$ , always for lines showing LWHM (Pa $\beta$ ) values above  $\sim 60\text{\AA}$ .

## 5. Concluding remarks

In this work we performed a search for very massive star candidates beyond the center of the massive stellar cluster NGC3603, which is known to be one of the most massive, dense and rich Galactic star-forming region, and believed to be a scaled version of the R136 star-

Table 5. Equivalent width (EW) and NIR line width (LW) measurements ( $\text{\AA}$ ), for sources in Table 2, with the exception of RFS10 for which we only have optical data, with the uncertainty on the quoted values varying from 10% to 15%.

Source	Pa $\beta$ (1) EW – LW	Br11 (2) EW – LW	He II (3) EW – LW	He I (4) EW – LW	Br10 (5) EW – LW	C IV (7-8) EW – LW	N V (9) EW – LW	He I (10) EW – LW	N III (11) EW – LW	Br $\gamma$ (12) EW – LW	He II (13) EW – LW
RFS1	1.3 – 8.8	0.85 – 32.5	0.62 – 21	0 – 0	1.8 – 25.9	1.1 – 54	-0.3 – 6.9	0 – 0	-0.88 – 19.2	em+abs	1.1 – 27.9
RFS2	-19.4 – 97.5	-4.2 – 117	0 – 0	0 – 0	-5.6 – 172	0.36 – 21.2	-0.72 – 35.5	0 – 0	-1.4 – 39.8	-15.7 – 126.7	-2.3 – 44.5
RFS3	-9.8 – 102.5	0 – 0	0 – 0	0 – 0	-2.5 – 71.9	0 – 0	0 – 0	0 – 0	-2.4 – 49.3	-4.1 – 91.4	-2.2 – 95.2
RFS4	2.4 – 17.2	1 – 29.4	0.7 – 14.4	0.2 – 8.5	1.9 – 21.9	-0.74 – 16.5	0 – 0	0 – 0	-1.6 – 30.2	3.1 – 54.2	1.2 – 25.5
RFS5	-17.7 – 65.5	-1.3 – 32.9	-0.59 – 31.6	0 – 0	-3.1 – 67	-0.82 – 26.9	-0.4 – 7.3	0 – 0	-2 – 25.2	-14.3 – 65	-2.5 – 28.5
RFS6	2.0 – 26.8	1 – 33.0	1.2 – 33.9	0.9 – 40.4	2.4 – 27.8	-1 – 24.8	0 – 0	0 – 0	-0.73 – 25.2	2.5 – 46.2	1.7 – 58.9
RFS7	-15.3 – 105	-2.2 – 86.4	0 – 0	0 – 0	-4.7 – 113	0 – 0	-0.9 – 43.9	0 – 0	-2.8 – 40.4	-3.2 – 40.4	-2.3 – 103
RFS8	-5.4 – 88.7	-1.9 – 42	0 – 0	0 – 0	-3.2 – 36.6	-5.7 – 128	0 – 0	0 – 0	-7.4 – 83.4	3.6 – 114	-1.8 – 66.1
RFS9	4.7 – 26.7	0.4 – 25.9	0.4 – 15.5	1.1 – 22.1	0.82 – 25.5	-0.28 – 14.7	0 – 0	0 – 0	-0.65 – 23.8	3.8 – 58	1 – 30
HD93129A	-5.7 – 99.0	-1 – 55	0 – 0	0 – 0	-6.2 – 105	-0.3 – 24	-0.2 – 13	0 – 0	-1.1 – 57	-6.3 – 124	0 – 0
WR20a	-26.7 – 85.0	-2.2 – 65.1	-11.1 – 175		-12.1 – 87.2				-2.2 – 78.3	-30.5 – 132	-6.9 – 91.4
WR20aa	-16.3 – 71.4	-2.2 – 57.3	-0.47 – 30		-5.3 – 54.8				-2.5 – 50	-18.6 – 129	-6.9 – 87.6
WR25	-22.5 – 70.0	-2.7 – 53.7	-4.5 – 87.6		-8.4 – 87.6				-3.4 – 56.8	-32.2 – 102.4	-12.3 – 87.6

Table 6. Equivalent width (EW) and line width (LW) measurements of selected optical lines ( $\text{\AA}$ ), for sources in Table 2, with the uncertainty on the quoted values ranging from 10% to 15%. We also show the values for HD 93129A taken from the optical spectrum in Roman-Lopes, Barbá & Morrel (2011)

Source	He I+II (1) EW – LW	N IV (2) EW – LW	He II (6) EW – LW	He I (10) EW – LW	He II (11) EW – LW	N V (12) EW – LW	N V (13) EW – LW	N III (14-1) EW – LW	N III (14-2) EW – LW	C IV (15) EW – LW	He II (16) EW – LW	H $\beta$ (17) Profile
RFS1	0.34 – 3	-0.46 – 4.5	0.57 – 4.4	0.06 – 1.02	0.71 – 4.1	0.23 – 2.1	0.18 – 2.5	-0.16 – 3.6	-0.23 – 3.8	-0.16 – 4.7	0.71 – 4.1	pure abs
RFS2	–	–	–	–	1.5 – 10.4	0.27 – 5.1	0.25 – 2.9	–	–	–	-7.5 – 20.6	P-Cygni
RFS3	0 – 0	-1 – 7.7	0.39 – 6.7	0 – 0	0.73 – 5.4	0.4 – 6.2	0.47 – 8.1	-0.2 – 14.3	0 – 0	0 – 0	-1.46 – 10.7	pure abs
RFS4	0 – 0	0 – 0	0.76 – 5.4	0 – 0	0.82 – 4.4	0 – 0	0 – 0	0 – 0	0 – 0	0 – 0	0.53 – 5.3	pure abs
RFS5	0.3 – 3.3	-1.2 – 3.6	0.33 – 3.6	0.14 – 3.3	0.52 – 4.4	0.38 – 3.2	0.26 – 3.2	-0.58 – 5.8	-0.72 – 4.8	0 – 0	-6.6 – 16.5	P-Cygni
RFS6	0 – 0	0 – 0	0.69 – 5.3	0.32 – 6	0.99 – 6.4	–	–	–	–	–	0.53 – 5.4	pure abs
RFS7	0.12 – 2.1	-0.8 – 2.8	0.34 – 3.8	0 – 0	0.56 – 3.7	0.2 – 2.3	0.17 – 2.6	-0.19 – 2.8	-0.36 – 3.3	-0.28 – 4.8	-4.3 – 12.8	P-Cygni
RFS8	0 – 0	-0.26 – 1.5	0.54 – 6	0 – 0	0.4 – 2.8	0.21 – 6	0.07 – 1.9	-0.4 – 6	-1.1 – 10	-0.7 – 11.2	-2.2 – 11.3	pure abs
RFS9	0.58 – 4.1	0 – 0	0.6 – 3.8	0.57 – 5.9	0.73 – 5	0 – 0	0 – 0	0 – 0	0 – 0	0 – 0	0.86 – 3.8	pure abs
RFS10	0.47 – 2.6	0 – 0	0.8 – 3.9	0.59 – 3.2	0.98 – 3.3	0 – 0	0 – 0	-0.41 – 2.9	-0.88 – 3.4	0 – 0	-1.28 – 4.4	pure abs
HD93129A	0.28 – 4.7	-1.5 – 5.5	0.35 – 4.6	0.13 – 5.8	0.8 – 4.7	0.7 – 4	0.67 – 4.7	-0.1 – 4.2	-0.09 – 4.5	-0.09 – 5.4	-4.2 – 24	pure abs

burst cluster in the LMC. Based on NIR colour and magnitude selection criteria applied to the 2MASS point source catalogue, the chosen stars were observed through a SOAR NIR and optical spectroscopic survey which confirmed the existence of several massive stars in isolation in the NGC3603 field.

From the analysis of the spectroscopic survey and related optical-NIR photometry, our main results are:

- Three new Galactic exemplars of the OIf\*/WN type, RFS2 (MTT58), RFS5 (WR42e) and RFS7, are confirmed in the periphery of NGC 3603. They are very young massive stars with probable initial masses well above  $100 M_{\odot}$  and estimated ages of about 1 Myr. RFS5 (O3If\*/WN6 -  $135 M_{\odot}$ ) appears to be a bit more massive than RFS2 and RFS7, both with estimated initial masses of  $\sim 115 M_{\odot}$ . Such results are in line with the estimated mass of NGC3603-C, the O3If\*/WN6 star placed in the core of the NGC 3603, which has an estimated mass of  $123\text{--}154 M_{\odot}$  and absolute visual magnitude  $M_V=-7.2$  (Crowther et al. 2010).
- Based on a Goodman blue-optical spectrum of RFS3 (MTT68), we may now confirm that it is indeed a highly reddened O2If\* star, the only other Galactic exemplar (besides HD93129A) known to date. Based on its position relative to a set of theoretical isochrons in a Hertzsprung-Russel diagram, we concluded that the new O2If\* star is probably one of the most massive ( $150 M_{\odot}$ ) and luminous ( $M_V=-7.3$ ) O-star in the Galaxy.
- The RFS1 blue-optical spectrum is a nearly clone of the prototype of the O2v class, the BI 253 star in the LMC (Walborn et al. 2002)), which makes RFS1 the first Galactic exemplar known to date. Based on its location on the Hertzsprung-Russel diagram, we found that it is a star with probable initial mass of  $80 M_{\odot}$ , and luminosity similar to the other O2v stars found in the LMC.
- The case of RFS8, a new Galactic O3.5 If\* star is quite intriguing. It is found well to the south of the NGC 3603 complex, in apparent isolation at a large radial angular center distance of  $29'$ , or equivalently, at a projected linear distance of about 62 pc. Based on its location in the H-R diagram and accordingly with the stellar evolutionary models, RFS8 probably had an initial mass of  $77 M_{\odot}$ . Its derived absolute magnitude  $M_V=-6.4$  is similar to that of the other O3.5If\* (Sh18) found in the NGC 3603's innermost region. The fact that a such high mass star is found well isolated in the field led us to speculate that it could have been expelled from the innermost parts of the complex.
- From the spectroscopic study and associated optical and NIR photometry, we were able to derive the values of the total to selective extinction ratio  $R_V$  and the corresponding

optical to NIR color excesses  $E(B-V)$ ,  $E(J-V)$ ,  $E(H-V)$  and  $E(K-V)$  for each star in our sample. Our results are consistent with an anomalous interstellar extinction law found on previous studies in the direction of the NGC 3603 region. In this sense, we found a radial dependence on the total to selective extinction ratio, with the associated  $R_V$  values decreasing as a function of  $r_c$  given by  $R_V = 3.881 - 0.014r_c$ .

- Based on the equivalent width (EW) and line width (LW) measurements made from the observed NIR spectroscopic lines, we constructed EW and  $EW \times LWHM$  comparative diagrams and found that the normal O-type stars can be easily separated from the OIf\* and OIf\*/WN type stars. Also, in the particular case of using only the K-band, it is possible not only to separate normal O-type stars from the OIf\* and OIf\*/WN types, but also to identify the majority of the OIf\*/WN type stars that present He II  $\lambda\lambda 21890$  and  $Br\gamma$  line width values satisfying simultaneously the condition  $EW(He II) < -2\text{\AA}$ , and  $EW(Br\gamma) < -12.5\text{\AA}$ , which correspond to a combined width  $W_\lambda(Br\gamma + He II) \sim 15\text{\AA}$ , about half of the value suggested by Crowther & Walborn (2011).

On the other hand, in the absence of K-band spectroscopic data, excellent results in the separation process are achieved using  $Pa\beta$  line measurements combined with those of H-band hydrogen Br10 and Br11 transitions. In this case the values defining the boundaries between OIf\* and OIf\*/WN stars correspond to the combined equivalent widths satisfying  $EW_\lambda(Br10 + Pa\beta) > 20\text{\AA}$ , and  $EW_\lambda(Br11 + Pa\beta) > 16\text{\AA}$ .

Finally, regarding approximate boundaries between subtypes analogous to the criterion using the He II  $\lambda 4686$  in the optical window (Crowther & Walborn 2011), the best choice in the NIR is that using the  $Pa\beta$  emission line for which we clearly see a transition boundary between OIf\* and OIf\*/WN stars occurring for  $EW(Pa\beta) \sim 12\text{\AA}$  and  $LWHM(Pa\beta)$  values above  $\sim 60\text{\AA}$ .

ARL thanks partial support from DIULS Regular project PR15143. GAPF is partially supported by CNPq and FAPEMIG. We thanks the anonymous referee by the careful reading of the manuscript. Her/his criticism was appreciated. We thanks the SOAR staff for the efficient support provided during the OSIRIS and Goodman observing runs. ARL thanks Dr. Nolan Walborn by stimulating discussions about optical spectra of O2V stars. ARL thanks Dr. Nidia Morrel by stimulating discussions on optical spectral classification of early-type stars. This publication makes use of data products from the Two Micron All Sky Survey, which is a joint project of the University of Massachusetts and the Infrared Processing and Analysis Center/California Institute of Technology, funded by the National Aeronautics and Space Administration and the National Science Foundation. IRAF is distributed by the



National Optical Astronomy Observatory, which is operated by the Association of Universities for Research in Astronomy (AURA) under a cooperative agreement with the National Science Foundation. This work is based [in part] on observations made with the Spitzer Space Telescope, which is operated by the Jet Propulsion Laboratory, California Institute of Technology under a contract with NASA. This research has made use of data obtained from the Chandra Source Catalog, provided by the Chandra X-ray Center (CXC) as part of the Chandra Data Archive. This research has made use of the VizieR catalogue access tool, CDS, Strasbourg, France. The original description of the VizieR service was published in A&AS 143, 23

*Facilities:* SOAR Telescope, OSIRIS, Goodman.

## REFERENCES

- Bestenlehner, J. M., Vink, J. S., Grafener, G., Najarro, F., Evans, C. J., Bastian, N., Bonanos, A. Z., Bressert, E., Crowther, P. A., Doran, E., Friedrich, K., Henault-Brunet, V., Herrero, A., de Koter, A., Langer, N., Lennon, D. J., Maiz Apellaniz, J., Sana, H., Soszynski, I., Taylor, W. D. 2011, A&A, 530, 14
- Bestenlehner, J. M., Grafener, G., Vink, J. S., Najarro, F., de Koter, A., Sana, H., Evans, C. J., Crowther, P. A., Henault-Brunet, V., Herrero, A., Langer, N., Schneider, F. R. N., Simon-Diaz, S., Taylor, W. D., Walborn, N. R. 2014, 570, 38
- Bonanos, A. Z., Stanek, K. Z., Udalski, A., Wyrzykowski, L., Zebrun, K., Kubiak, M., Szymanski, M. K., Szewczyk, O., Pietrzynski, G., Soszynski, I. 2004, ApJ, 611, 33
- Bressan, A., Marigo, P., Girardi, L., Salasnich, B., Dal Cero, C., Rubele, S., Nanni, A. 2012, MNRAS, 427, 127
- Chini, R., Kruegel, E. 1983, A&A, 117, 289
- Chini, R., Wargau, W. F. A&A, 227, 213
- Crowther, Paul A., Hadfield, L. J., Clark, J. S., Negueruela, I., Vacca, W. D. 2006, MNRAS, 372, 1407
- Crowther P. A., Schnurr O., Hirschi R., Yusof N., Parker R. J., Goodwin S. P., Kassim H. A. 2010, MNRAS, 408, 731
- Crowther, P., Walborn, N. 2011, MNRAS, 416, 1311

- de Koter, A., Heap, S. R., Hubeny, I. 1997, *ApJ*, 477, 792
- Fedorov, P. N., Akhmetov, V. S., Bobylev, V. V., Gontcharov, G. A. 2011, *MNRAS*, 415, 665
- Fitzpatrick, Edward L. 1999, *PASP*, 111, 63
- V. V. Gvaramadze & A. Gualandris 2011, *MNRAS*, 410, 304
- Gvaramadze, V. V., Kniazev, A. Y., Chene, A.-N.; Schnurr, O. 2013, *MNRAS*, 430, L20
- Hanson, M. M., Conti, P. S., Rieke, M. J. 1996, *ApJS*, 107, 281
- Hanson, M. M., Kudritzki, R.-P., Kenworthy, M. A., Puls, J., Tokunaga, A. T. 2006, *ApJS*, 161, 154
- Hur, H., Sung, H., Lim, B. 2014, *ASPC*, 482, 239
- Lamers, H. J. G. L. M., & Cassinelli, J. P. 1999, *Introduction to stellar winds* (Cambridge University Press)
- Martins, F., Schaerer, D., Hillier, D. J., Meynadier, F., Heydari-Malayeri, M., Walborn, N. R. 2005, *A&A*, 441, 735
- Martins, F., Plez, B. 2006, *A&A*, 457, 637
- Massey, P., Puls, J., Pauldrach, A. W. A., Bresolin, F., Kudritzki, Rolf P., Simon, T. 2005, *ApJ*, 627, 477
- Melena, M. W., Massey, P., Morrell, N.I., Zangari, A. M. 2008, *AJ*, 135, 878
- Melnick, J., Tapia, M., Terlevich, R. 1989, *A&A*, 213, 89
- Moffat, A. F. J., Shara, M. M., Potter, M. 1991, *AJ*, 102, 642
- Moffat, A. F. J., Corcoran, M. F., Stevens, I. R., Skalkowski, G., Marchenko, S. V., Mcke, A., Ptak, A., Koribalski, B. S., Brenneman, L., Mushotzky, R., Pittard, J. M., Pollock, A. M. T., Brandner, W. 2002, *ApJ*, 573, 191
- Neckel, T., Chini, R. 1981, *A&A*, 45, 451
- Niemela V. S., Gamen R. C., Barba R. H., Fernandez L. E., Benaglia P., Solivella G. R., Reig P., Coe M. J. 2008, *MNRAS*, 389, 1447
- Ochsenbein, F.; Bauer, P.; Marcout, J. 2000, *A&AS*, 143, 23

- Pandey, Anil K., Ogura, Katsuo, Sekiguchi, Kaz 2000, PASJ, 52, 847
- Rauw, G., Vreux, J.-M., Gosset, E., Hutsemekers, D., Magain, P., Rochowicz, K. 1996, RMxAC, 5, 108
- Rauw, G., De Becker, M., Nazao, Y., et al. 2004, A&A, 420, L9
- Repolust, T., Puls, J., Herrero, A. 2004, A&A, 415, 349
- Roeser, S., Demleitner, M., Schilbach, E. 2010, AJ, 139, 2440
- Roman-Lopes, A. 2009, MNRAS, 398, 1368
- Roman-Lopes, Barba, R. & Morrell, N. 2011, MNRAS, 416, 501
- Roman-Lopes, A. 2012, MNRAS, 427, 65
- Roman-Lopes, A. 2013a, MNRAS, 433, 712
- Roman-Lopes, A. 2013b, MNRAS, 435, 73
- Romano, P., Campana, S., Mignani, R. P., Moretti, A., Mottini, M., Panzera, M. R., Tagliaferri, G. 2008, A&A, 488, 1221
- Rosslowe, C. K., Crowther, P. A. 2015, MNRAS, 447, 2322
- Sabín-Sanjulián, C., Simón-Díaz, S., Herrero, A., Walborn, N. R., Puls, J., Maíz Apellíniz, J., Evans, C. J., Brott, I., de Koter, A., Garcia, M., Markova, N., Najarro, F., Ramírez-Agudelo, O. H., Sana, H., Taylor, W. D., and Vink, J. S. 2014, A&A, 564, 39
- Sana, H., Gosset, E., Evans, C. J. 2009, MNRAS, 400, 1479
- Schnurr, O., Casoli, J., Chenè, A.-N., Moffat, A. F. J., St-Louis, N. 2008, MNRAS, 389, 38
- Schnurr, O., Moffat, A.F.J., Villar-Sbaffi, A., St-Louis, N., Morrell, N. 2009, MNRAS, 395, 823
- Shara, M. M., Smith, L. F., Potter, M., Moffat, A. F. J. 1991, AJ, 102, 642
- Shara, Michael M., Moffat, Anthony F. J., Gerke, Jill, Zurek, David, Stanonik, Kathryn, Doyon, Ren, Artigau, E., Drissen, L., Villar-Sbaffi, A. 2009, AJ, 138, 402
- Simon, K. P.; Kudritzki, R. P.; Jonas, G.; Rahe, J. 1983, A&A, 125, 34

- Skrutskie, M. F., Cutri, R. M., Stiening, R., Weinberg, M. D., Schneider, S., Carpenter, J. M., et al. 2006, *AJ*, 131 1163
- Smith, N. & Conti, P. S. 2008, *ApJ*, 679, 1467
- Sota, A., Maíz Apellániz, J., Walborn, N. R., Alfaro, E. J., Barbá, R. H., Morrell, N. I., Gamen, R. C., Arias, J. I. 2011, *ApJS*, 193, 24
- Sota, A., Maíz Apellániz, J., Morrell, N. I., Barbá, R. H., Walborn, N. R., Gamen, R. C., Arias, J. I., Alfaro, E. J. 2014, *ApJ*, 211, 10
- Sung, H., Bessell, M. S. 2004, *AJ*, 127, 1014
- Taresch, G., Kudritzki, R. P., Hurwitz, M., Bowyer, S., Pauldrach, A. W. A., Puls, J., Butler, K., Lennon, D. J., Haser, S. M. 1997, *A&A*, 321, 531
- Townsley, L. K., Broos, P. S., Garmire, G. P., Bouwman, J., Povich, M. S., Feigelson, E. D., Getman, K. V., Kuhn, M. A. 2014, *ApJS*, 213, 1
- Vink, J. S., Heger, A., Krumholz, M. R., Puls, J. et al. 2015, *Highlights of Astronomy*, 16, 51
- Walborn, N. 1982, *ApJ*, 254, 15
- Walborn, N. & Blades, C. 1997, *ApJS*, 112, 457
- Walborn, N., Howarth, I. D., Lennon, D. J., Massey, P., Oey, M.S., Moffat, A. F. J., Skalkowski, G., Morrel, N. I., Drissen, L., Parker, J. W. 2002, *AJ*, 123, 2754
- Walborn, N., Sana, H., Simón-Díaz, S., Maíz Apellániz, J., Taylor, W. D., Evans, C. J., Markova, N., Lennon, D. J., de Koter, A. 2014, *A&A*, 564, 40
- W. Wegner 2005, *MNRAS*, 371, 185
- XMM-Newton Survey Science Centre, C. 2013, *VizieR Online Data Catalog*, 9044, 0
- Zacharias, N., Monet, D. G., Levine, S. E., Urban, S. E., Gaume, R., Wycoff, G. L. 2004, *AAS*, 205, 4815
- Zacharias, N., Finch, C. T., Girard, T. M., Henden, A., Bartlett, J. L., Monet, D. G., Zacharias, M. I. 2013, *AJ*, 145, 44